NORTHWESTERN UNIVERSITY

Myeloproliferative Neoplasms: From Biology to Targeted Therapeutics

A DISSERTATION

SUBMITTED TO THE GRADUATE SCHOOL

IN PARTIAL FULLFILLMENT OF THE REQUIREMENTS

For the degree

DOCTOR OF PHILOSOPHY

Field of Life Sciences

By

Christian Marinaccio

EVANSTON, ILLINOIS

March 2021

ABSTRACT

The BCR-ABL negative Myeloproliferative Neoplasms (MPNs) are clonal hematopoietic stem-cell disorders characterized by abnormal proliferation of differentiated myeloid lineages. MPNs include 3 clinically distinct disorders: Polycythemia Vera (PV), Essential Thrombocythemia (ET) and Primary Myelofibrosis (PMF). 95% of MPNs are characterized by driver mutations in Janus Kinase 2 (*JAK2*), Thrombopoietin receptor (*MPL*) and Calreticulin (*CALR*) which each lead to constitutive activation of the JAK-STAT signaling pathway.

PMF is the most aggressive subtype of MPN, characterized by elevated white blood counts, splenomegaly and bone marrow fibrosis. The median survival of these patients in the high-risk category is 16 months, and the two only current FDA approved targeted therapies for PMF are Ruxolitinib and Fedratinib, JAK2 inhibitors that provide therapeutic benefits, but are limited by toxicity and eventual resistance. A striking feature of PMF is the presence of an expanded population of atypical megakaryocytes which are thought to have a major role in the development of the disease. We previously showed that targeting megakaryocytes with the Aurora Kinase A (AURKA) inhibitor Alisertib resulted in reduced disease burden and bone marrow fibrosis in preclinical mouse models of MPN. The first part of this dissertation describes the results of a multi-center Phase I clinical trial that was carried out at Northwestern University in collaboration with Mayo Clinic and Miami University evaluating the safety and preliminary clinical activity of Alisertib in the treatment of PMF.

We show that Alisertib has on-target effects on the megakaryocyte lineage, including normalization of bone marrow megakaryocyte morphology and decreased bone marrow fibrosis.

Furthermore, MPNs are characterized by progression to an aggressive form of Acute Myeloid Leukemia named Blast-Phase MPN (MPN-BP). MPN patients transform to MPN-BP with rates of 10-20%, 2-5% ad 1-4% in PMF, PV and ET, respectively. MPN-BP has a dismal prognosis with a median survival of only 3-5 months, and the drivers of transformation of MPNs to MPN-BP are largely unknown. In the second part of this dissertation, we describe the involvement of Serine Threonine Kinase 11/Liver Inducible Kinase 1 (STK11/LKB1) in the progression of MPN to MPN-BP. With my collaborators I show that loss of STK11/LKB1 in MPN cells is associated with enhanced self-renewal in-vitro and rapid lethality in a mouse model of MPN. Furthermore, we show that loss of STK11/LKB1 cause increase of mitochondrial reactive oxygen species (mitoROS) that lead to stabilization of hypoxia inducible protein 1α (HIF1α). Finally, we provide evidence of increased HIF1α stabilization and STK11/LKB1 loss in human MPN-BP.

Acknowledgements

When I first arrived in Chicago coming from a small town in southern Italy, I was excited and scared at the same time to begin a PhD in a big US institution like Northwestern University. Now after more than 5 years I can say that earning it was one of the hardest things I achieved in my life so far.

I am incredibly grateful to my advisor and mentor Dr. John Crispino for giving me the opportunity to grow in his laboratory and pursue research in experimental hematology, a field that fascinated me since I was a masters' degree student in Italy. I was inspired by his determination and his capacity to bring the best out of his trainees. I have learned so much in these 5 years thanks to his guidance, and I will keep continue to seek his advice in the years to come, as the path to scientific independence is still long and full of new challenges.

I want to thank the members of Crispino lab who were supportive throughout the years and helped me progress through many obstacles. I also thank all our collaborators that I was fortunate to meet along the road: Dr. Ayalew Tefferi, Dr. Naseema Gangat, Dr. Terra Lasho, Dr. Ross Levine, Dr. Raajit Rampal, Dr. Grant Challen and Dr. Hamza Celik, and their collaborators. They provided invaluable help and feedback to push my projects forward.

I want to thank my committee members, Dr. Navdeep Chandel, Dr. Brian Mitchell, Dr. Issam Ben-Sahra, and Dr. Panagiotis Ntziachristos. I thank them for being available to discuss my

projects and offer extremely valuable advice about experiments and ideas. I am grateful for their additional mentorship which was key to get me to the finish line.

Special thanks goes to fellow Italians in Chicago, Dr. Eleonora Forte, Dr. Roberto Ponciroli, Dr. Daniele Rosso for their support. And thanks to Dr. Andrea Piunti, that like the others, made my life easier by making me laugh so much throughout the years. Those are friendships that I will cherish wherever I go in the future.

This thesis would not have been possible without the support of my wife Francesca. We integrated together in a new country and a new culture, which is always a tricky part for internationals living abroad. Even in the darkest moments she was there comforting me and cheering me up, urging me to not give up. Not everyone would be willing to follow a scientist-in-progress to another continent. Despite the difficulties we always pulled through.

Last but not least I want to thank my family in Italy, my mother Silvia, my father Francesco and my sister Sabrina. I know how hard it was for them to see me moving from Bari to Chicago more than 8000 Km away from home but at the same time they did everything they could to make sure I would not feel too lonely and missing Italy too much, especially the first year when I was alone in Chicago. Even though they don't understand much English or how a PhD works, they always asked about my work and wanted to know about every little detail. They motivated me so much to do my best every day during this PhD.

In the end a critical part of this work was done during the Covid-19 pandemic that was tough everywhere on the planet. I hope that all PhD researchers around the world will carry on and be successful despite this unprecedented and unique event that affected our lives.

PREFACE

Chapters II is derived from the article "Aurora Kinase A Inhibition Provides Clinical Benefit, Normalizes Megakaryocytes, and Reduces Bone Marrow Fibrosis in Patients with Myelofibrosis: A Phase I Trial" published in *Clinical Cancer Research* in 2019.

Chapter III is derived from the article "LKB1/STK11 is a tumor suppressor in the leukemic transformation of myeloproliferative neoplasms" accepted for publication in *Cancer Discovery* in 2021.

Table of Contents

List of Figures

List of Tables

CHAPTER I

INTRODUCTION TO THE MYELOPROLIFERATIVE NEOPLASMS (MPNs)

Hematopoiesis is a complex process that provides the body with the cellular components of blood and immune system. During the lifetime of an individual, hematopoiesis takes place primarily in the bone marrow where a reservoir of hematopoietic stem cells (HSCs) give rise to committed progenitors and a new hematopoietic stem cell through asymmetric division. There are two types of hematopoietic tissue: the myeloid compartment that produces mature monocytes, granulocytes, erythroid cells and megakaryocytes in the bone marrow and the lymphoid compartment that produces NK, T and B lymphocytes which complete their maturation in the lymph nodes, spleen and thymus.

The bone marrow is a highly proliferative tissue, and hemopoiesis is a coordinated process that requires multiple interactions between the hematopoietic stem and progenitor cells (HSPCs), stromal cells and growth factors which direct the cell fate and the production of the final cell type. Studies have suggested that the total number of stem cell divisions is correlated to cancer risk, and the stochastic effects of DNA replication[1,2] can contribute to the acquisition of pathogenic somatic mutations in HSCs which cause development of hematopoietic malignancies.

1.1 Myeloproliferative Neoplasms

The 2016 World Health Organization (WHO) system for the classification of tumors of the hematopoietic and lymphoid tissue defines three major distinct clinical entities characterized by driver mutations in the JAK-STAT pathway: Polycythemia Vera (PV), Essential

Thrombocythemia (ET) and Primary Myelofibrosis (PMF). At least another four clinical entities are listed as MPN: Chronic Myeloid Leukemia (CML), which is characterized by the presence of the BCR-ABL1 mutation, Chronic Neutrophilic Leukemia (CNL) which cause clonal proliferation of mature neutrophils harboring mutations in the granulocyte colony-stimulating factor 3 receptor (*CSF3R*), Chronic Eosinophilic Leukemia not otherwise specified (CEL-NOS), characterized by clonal eosinophilia associated with cytogenetic abnormalities including trisomy of chromosome 8, and MPN, unclassifiable (MPN-U) that includes MPN neoplasms that are not clearly classifiable in the other mentioned categories[3]. This introduction will focus on the three major MPN subcategories and their shared abnormally activated JAK-STAT signaling pathway.

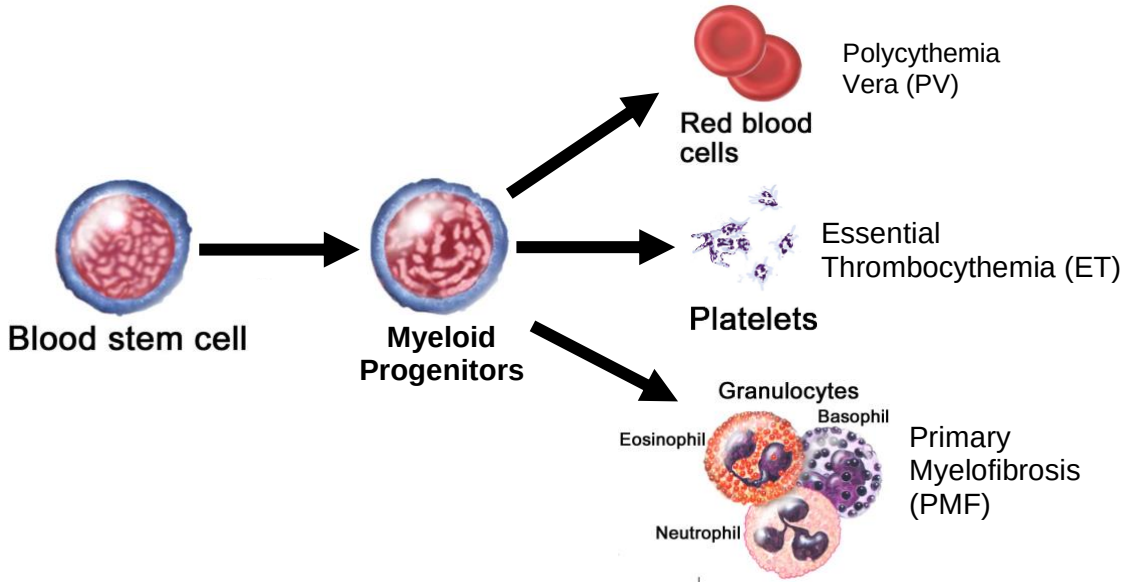

Figure 1 – Myeloproliferative Neoplasms

1.2 Polycythemia Vera

Polycythemia Vera (PV) is characterized by excessive production of mature red blood cells. The prevalence of PV has been estimated to be 44 to 57 cases per 100,000 people[4], with a large proportion of underestimated cases that may be asymptomatic or latent based on large population surveys[5]. PV diagnosis can occur in all age groups with a median age at diagnosis of 61 years with a gender skew towards men[6]. A diagnosis of PV is confirmed by the presence of the somatic *JAK2*^{V617F} mutation, which is present in >95% of PV patients, and increased red cell mass with values of hemoglobin (Hgb) greater than 16.5 g/dL in women and greater than 18.5 g/dL in men[7]. Pathology of bone marrows core biopsies from PV patients exhibit marked expansion of the red cell lineage along with expansion of the megakaryocytic lineage[3].

PV patients present with a symptom burden that affects quality of life such as fatigue, insomnia and itching with thrombosis as the most common and severe complication. Thrombotic events in PV patients are implicated in 37% of deaths[8] with a predominance of cerebrovascular arterial thrombosis[9]. Venous thrombosis is less common but adversely affects survival[9].

Therapeutic options for PV patients aim to reduce thrombosis risk and symptom burden. One of the most common treatments for PV patients is phlebotomy, which is used to reduce the red cell mass. Cytoreductive therapy is indicated for high-risk patients with a history of thrombosis and involves the use of hydroxyurea (HU). In addition to these treatments, targeted therapies involving JAK-STAT pathway inhibition through Ruxolitinib or

Fedratinib, or Pegylated Interferon Alpha (peg-IFN-α) provide clinical benefit. However, patients ultimately develop resistance to JAK inhibitors, and toxicity remains the main side effect of peg-IFN-α[7].

1.3 Essential Thrombocythemia

Essential Thrombocythemia (ET) is characterized by marked increase in platelets derived from an expansion of the megakaryocyte lineage. ET has a prevalence of 38 to 57 cases per 100,000 people[4]. As for PV, the diagnosis of ET can occur in all age groups with a median age at diagnosis of 58 years[10]. ET patients present with a platelet count greater than 450 x 10^9/L, evidence of megakaryocyte proliferation with large and mature morphology in the bone marrow and mutations in *JAK2*, *CALR* or *MPL*[3].

ET patients have variable symptoms including migraines, headache and dizziness and show an elevated risk of thrombosis[11], particularly in the hepatic vein and bleeding due to platelet dysfunction or acquired von Willebrand syndrome, which occurs more commonly in patients with extreme thrombocytosis[12]. Therapeutic strategies for ET patients include cytoreductive therapy with hydroxycarbamide (HC), Anagrelide, an inhibitor of cyclic AMP phosphodiesterase which can inhibit megakaryocyte differentiation and proliferation. Moreover, inhibition of the JAK-STAT pathway with Ruxolitinib was investigated in a small group of ET patients refractory to HC and demonstrated improvements in symptoms burden and splenomegaly[13].

1.4 Primary Myelofibrosis

Primary Myelofibrosis (PMF), with a prevalence of 4 to 6 cases per 100,000 people[4], is the most aggressive MPN subtype characterized by progressive bone marrow fibrosis, leukocytosis and presence of atypical dysplastic megakaryocytes. PMF patients have several clinical manifestations including hepatosplenomegaly, severe anemia, thrombosis and bleeding[14]. PMF can occur de novo or constitute a progression from previously diagnosis of PV or ET where a bone marrow fibrosis of grade 2-3 or grade 3-4 is present. Based on the DIPSS-plus prognostic system PMF can be subdivided in 4 risk stratifications: low risk, intermediate-1 risk, intermediate-2 risk and high risk with a median survival of 15.4 years, 6.5 years, 2.9 years and 1.3 years, respectively[14].

In terms of therapeutic options, the JAK2 inhibitors Ruxolitinib and Fedratinib are the only targeted therapies approved for the treatment of PMF. These drugs lead to a significant reduction of spleen volume which correlated with symptomatic improvement[15,16]. However, JAK inhibitors do not consistently decrease allele burden or the degree of bone marrow fibrosis. Morevoer, discontinuation of Ruxolitinib therapy is observed for 75% of the patients at 5 years[17]. One mechanism for development of ruxolitinib resistance involve heterodimerization of JAK2 and JAK1 leading to activation of the JAK-STAT pathway by interactions of JAK2 *in trans* with other JAK kinases. Increased phosphorylation of JAK1 was observed both in ruxolitinib resistant cell lines as well as in granulocytes from ruxolitinib treated patients[18].

1.5 The JAK-STAT signaling pathway

The three main driver mutations in MPNs result in constitutive activation of the JAK-STAT signaling pathway. This signaling pathway leads to the activation of transcription following stimulation with cytokines and growth factors. Under normal conditions, intracellular activation of the STAT transcription factors is achieved by binding of erythropoietin (EPO) or thrombopoietin (TPO) to the EPO receptor (EPO-R) or the thrombopoietin receptor (MPL), respectively. Binding of these cytokines induce multimerization of receptor subunits. In the cytoplasm, domains of the receptors subunits are associated with the JAK2 tyrosine kinase which are activated by transphosphorylation thanks to the receptor multimerization upon ligand binding. Once activated, the JAK2 kinase phosphorylates its major substates: STAT proteins, which are transcription factors that are present in the cytoplasm in an inactive form. The activated JAK2 kinase phosphorylates STATs on a conserved tyrosine residue located close to the C-terminal domain which allows for dimerization through the SH2 domain of two STAT proteins. The STAT dimer will then translocate to the nucleus and bind to regulatory sequences on DNA to activate or repress transcription of its target genes[19].

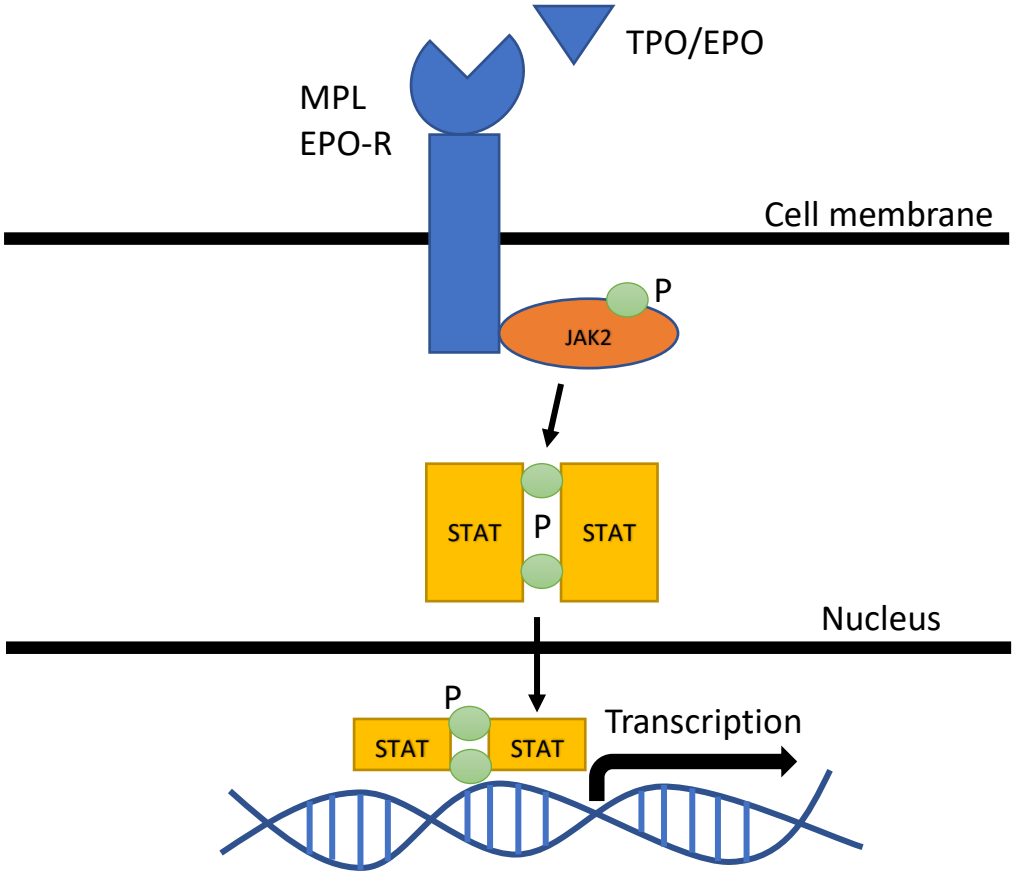

Figure 2 – The JAK-STAT signaling pathway.

This physiologic activation of the JAK-STAT pathway is disrupted in MPNs by three common recurring mutations. The main mutation that causes PV in 95% of the patients with PV and over 50% of the patients with ET and PMF[20] is a G to C transition at codon 617 of the JAK2 protein which causes a valine to phenylalanine substitution (*JAK2*^{V617F}). This mutation disrupts the JH2 pseudokinase domain resulting in constitutive activation of JAK2 and consequent increase of STAT5 phosphorylation[21]. The second MPN driver mutation affects the thrombopoietin receptor MPL upstream of the JAK2 protein. A transition of G to T causes a substitution from tryptophan to leucine at codon 515 of MPL (*MPL*^{W515L})[22], which

is located in the transmembrane domain of the protein within an amphipathic motif important for preventing spontaneous activation of the receptor[23]. Similar to JAK2, the mutation constitutively activate the pathway resulting in increased STAT3 and STAT5 phosphorylation. The third recently discovered mutation in MPNs is in the *CALR* gene, which encodes a calcium binding protein with protein chaperone functions that localizes to the endoplasmic reticulum (ER). Whole exome sequencing demonstrated deletions (*CALR*del type I) or insertions (*CALR*ins type II) in exon 9 of *CALR* resulting in a reading frameshift that abrogates the ER-targeting KDEL sequence[20,24]. Similar to the other two main mutations, the CALR mutant protein induces increased phosphorylation of STAT proteins and constitutive activation of the JAK-STAT pathway[25]. The molecular mechanism by which the mutant CALR protein induces activation of the JAK-STAT pathway involves increased transport of mutant CALR to the cell surface due to the absence of the ER retention signal and consequent activation of the JAK-STAT pathway through binding of mutant CALR to the thrombopoietin receptor MPL[26].

1.6 Role of the Megakaryocyte lineage in PMF

One of the hallmarks of PMF due to constitutively active JAK-STAT signaling is the expansion of the megakaryocytic lineage. Megakaryocytes are platelet producing cells in the body which can differentiate from a HSC-derived bipotent progenitor called megakaryocyte-erythroid progenitor (MEP) or differentiate directly from platelet-primed HSCs[27] by progressive accumulation of DNA content (polyploidization) achieved through the

endomitosis process. Commitment to the megakaryocyte lineage is dependent on the JAK-STAT pathway through signal transduction events involving TPO and its receptor MPL[28]. At the gene expression level, the transcription factor GATA1 is crucial for proper differentiation of megakaryocyte and erythroid progenitors[29]. GATA1 in conjunction with FLI1 and ETS1 lead to the expression of megakaryocyte specific receptors MPL, CD41 and CD42a[30]. During maturation of megakaryocytes, GATA1 also induces expression of the transcription factor NFE2, which activates the expression of several genes related to proplatelet formation such as *TUBB1*, encoding for the tubulin β-1 chain, a major component of microtubules[31,32].

Bone marrows of PMF patients show increased number of clustered, dysplastic atypical megakaryocytes with hyperchromatic and hypolobulated nuclei. *In-vitro* culture of human $CD34^+$ progenitors from PMF patients leads to increased outputs of $CD41^+$ megakaryocytes compared to healthy donors with defects in proplatelet formation[33]. This expansion is recapitulated in *in-vivo* mouse models of PMF where transplantation of c-kit^+ mouse progenitors with the MPL^{W515L} driver mutation leads to increased numbers of atypical megakaryocytes in the bone marrow and spleen[22]. Moreover, megakaryocytes from the mouse model and the human PMF display reduced levels of GATA1 expression at the protein level, which leads to differentiation abnormalities and decreased polyploidization[34]. Megakaryocytes have been linked to development of bone marrow fibrosis in mouse models. Specifically, overexpression of murine TPO in bone marrow cells and their transplantation in lethally irradiated mice (Tpo^{high} mice) leads to MPN development with megakaryocyte

hyperplasia, bone marrow fibrosis and osteosclerosis[35]. Furthermore, transgenic mice engineered to express low levels of GATA1 ($GATA1^{low}$ mice) also develop megakaryocyte hyperplasia and progressive accumulation of bone marrow fibrosis is seen with aging[36]. In both models, increased expression of transforming growth factor β (TGFβ) is present and contributes to fibrosis development. Of note, overexpression of murine TPO in bone marrow cells derived from TGFβ1 knockout mice lead to development of MPN but reduced levels of bone marrow fibrosis[37]. In $GATA1^{low}$ mice, inhibition of TGFβ1 signaling through TGFβ1 receptor type I normalized megakaryocyte development and reduced bone marrow fibrosis[38].

The importance of the megakaryocyte lineage in sustaining abnormal hematopoiesis in MPNs makes it amenable for targeted therapeutics which could complement the beneficial effects seen with JAK-STAT inhibition. Moreover, given the involvement of abnormal megakaryocytes in the development of bone marrow fibrosis, improvement of their differentiation status could prevent progression of PV and ET to the more aggressive post-PV and post-ET myelofibrosis.

1.7 Introduction to Blast-Phase MPN and the tumor suppressor STK11/LKB1

The natural history of MPNs occurs through decades with several complications that can modify the course of the disease. Common complications of PV and ET include the occurrence of thrombohemorrhagic events or disease progression to post-ET or post-PV myelofibrosis (MF), which can then advance to a spent phase of the disease characterized by bone marrow failure. Patients from each MPN phenotype can also progress to an

aggressive form of acute myeloid leukemia termed Blast Phase MPN (MPN-BP) whose genetic causes are not well understood.

The following paragraphs will describe characteristics of MPN-BP and introduce LKB1/STK11, a tumor suppressor that we found to be involved in the progression of MPN to MPN-BP.

1.8 Presentation and characteristics of MPN-BP

MPN-BP is characterized by the presence of 20% or more leukemic blasts in the peripheral blood or bone marrow[39]. The leukemic blasts in most of the cases originate from the myeloid lineage and rarely originate from the lymphoid lineage. The morphologic and cytogenetic characteristics of MPN-BP are different from primary de-novo acute myeloid leukemia (AML). The most common subtypes of MPN-BP according to the French-American-British classification (FAB) of AML are erythroleukemia (FAB-M6) and megakaryoblastic leukemia (FAB-M7)[40,41]. Since JAK-STAT activation plays a key role in both erythroid cells and megakaryocytes, the preponderance of FAB-M6 and FAB-M7 subtypes suggests leukemic transformation from a clone retaining MPN driver mutations, although MPN-BP arising from clones without MPN driver mutations have been reported[42].

The incidence of AML in patients that progress from PV or ET to post-PV MF or post-ET MF is similar to the incidence observed in de-novo PMF although PV and ET patients can develop MPN-BP directly without progression to a fibrotic stage[41,43]. At the time of

presentation, most MPN-BP patients display a complex karyotype rather than a normal karyotype with the presence of structural abnormalities involving most chromosomes[44]. Common mutations in MPN-BP involve driver mutations that activate the JAK-STAT pathway such as *JAK2*, *MPL* or *CALR*, in epigenetic regulators such as *ASXL1*, *TET2*, *JARID2* and in tumor suppressors such as *TP53*[45-47]. A DNA sequencing study focusing on *ASXL1*, *TET2*, *IDH1* and *JAK2* found combinations of *JAK2* mutations with *ASXL1*, *TET2* and *IDH1* suggesting they are not mutually exclusive[45]. Furthermore, the study reported patients with *ASXL1* mutations present at both MPN and MPN-BP stage of the disease, while mutations in *TET2* were acquired in the MPN-BP phase of the disease. Although clonal evolution of MPN to MPN-BP involves acquisition of new mutations, loss of the *JAK2-V617F* MPN driver mutation in leukemic blasts from MPN-BP patients have been reported, suggesting the presence of mutant clones independent from the MPN clones harboring JAK-STAT driver mutations[42].

1.8.1 Leukemic transformation from PV

Common treatments for PV include the anti-neoplastic drugs pipobroman and chlorambucil which act as alkylating agents. These agents have been connected with higher risk of leukemic transformation from PV, while phlebotomy, hydroxyurea (HU) and interferon treatments were not associated with leukemic transformation[48]. Combination of HU with alkylating agents also resulted in higher risk of transformation[48]. Additional risk factors include older age, leukocytosis and abnormal karyotype[9,49].

A study evaluating 1545 patients with PV quantified the cumulative incidence of post-PV MPN-BP with death as a competing risk at 2.3% at 10 years and 7.9% at 20 years. In the study, a total of 50 patients progressed to MPN-BP[9]. In another study on 133 patients with PV, targeted deep sequencing identified mutations in *ASXL1, SRSF2* and *IDH2* as adverse variants influencing leukemia-free survival in multivariate analysis[50].

1.8.2 Leukemic transformation from ET

Expansion and morphological abnormalities of the megakaryocyte lineage are common features of ET. These features are shared with a recently defined stage of PMF called prefibrotic PMF which is characterized megakaryocyte abnormalities and increased white blood counts without fibrosis[51,52]. Earlier studies have initially quantified the risk of leukemic transformation from ET in a range from 2.6% to 9.7% at 10 years[53,54]. A more recent study evaluated 891 patients with initial ET diagnosis and then excluded patients that had a revised diagnosis of prefibrotic PMF. The study revealed a much lower risk of leukemic transformation from ET at less than 1% at 10 years[55].

A study on 386 patients with ET found no significant correlation between the incidence of leukemic transformation and cytotoxic therapy indicating that treatment with single agents such as HU or busulfan do not result in an increase of risk of transformation to MPN-BP[56].

1.8.3 Leukemic transformation from PMF

PMF has the highest risk of transformation to MPN-BP, with an incidence of 10% to 20% at 10 years[40,43,57]. Several risk factors for leukemic transformation in patients with PMF have been identified. A study on 311 patients with PMF identified peripheral blood blast count >3% and a platelet count < 100 x 10^9/L as independent prognostic factors for leukemia free survival and quantified the risk of transformation at 6% without both risk factors and 18% with one or both the mentioned risk factors[58]. The study also evaluated the effect of therapy on leukemia-free survival and concluded that treatment with erythropoiesis stimulating agents increased the risk of transformation while treatment with HU, IFN-α, thalidomide and lenalidomide did not significantly increase risk of leukemic transformation[58].

Cytogenetic abnormalities have also been reported as a risk factor for leukemic transformation. A study on 793 patients with PMF evaluated leukemia-free survival based on abnormal karyotype and concluded that monosomal karyotypes, defined as the presence of 2 or more autosomal monosomies or a single autosomal monosomy with structural abnormalities, were associated with higher 2-year rate (29.4%) of leukemic transformation[59]. The effect of driver mutation status on leukemic transformation risk has also been reported in a study on 428 patients with PMF. The study found that leukemia-free survival was worse in triple-negative patients compared with *CALR*, *JAK2* and *MPL* mutant patients, while *CALR* mutant patients showed the lower risk of leukemic transformation when compared with triple-negative patients[60].

1.9 The tumor suppressor STK11/LKB1

Serine Threonine Kinase 11 (STK11), also known as Liver Kinase B1 (LKB1) is a protein kinase involved on regulation of cell metabolism, growth control and cell polarity through phosphorylation of its main target AMP-activated protein kinase (AMPK) and 12 other kinases structurally related to AMPK. This section will describe STK11 functions and role as a tumor suppressor in cancer.

1.9.1 STK11/LKB1 structure and biochemical properties

The STK11/LKB1 protein is encoded by the *STK11* gene on chromosome 19 in humans and by the *Stk11* gene on chromosome 10 in mice. The human gene produces a protein of 436 amino acids with the protein kinase domain extending from amino acid 50 to 319[61]. STK11 has two known splicing variants that differ mainly in the carboxy-terminal amino acids of the protein. STK11/LKB1 possess a nuclear localization signal (NLS) which localizes the protein to the nucleus. Mutants of STK11/LKB1 in the NLS are still able to suppress growth in overexpression systems indicating that its function is primarily exerted in the cytosolic fraction[62]. STK11/LKB1 is exported to the cytoplasm upon association with the pseudo-kinase STRAD (STRADα or STRADβ) and scaffold protein MO25 (MO25α or MO25β) to form a heterotrimeric complex necessary for STK11/LKB1 kinase activity. Heterotrimeric complexes can be isolated from mammalian 293 expression systems and the three complexes are present in similar stoichiometry indicating an high affinity of the individual components of the complex for each other[63]. Furthermore, the importance of complex formation for

STK11/LKB1 activation is highlighted by the presence of *STK11* mutations in Peutz-Jegher Syndrome (PJS) that abolish interaction with MO25 and STRAD and decrease STK11/LKB1 kinase activity[64].

In recent studies, regulation of STK11/LKB1 function by several types of post-translational modifications have been reported. Autophosphorylation of STK11/LKB1 at T185 and T402 increases its kinase activity[65] while phosphorylation of STK11/LKB1 at S299 by Aurora-A and S325 by ERK suppresses LKB1-AMPK interaction in non-small cell lung cancer (NSCLC) cell lines[66,67]. STK11/LKB1 is also ubiquitinated at K41, K44, K48, K62 and K63 by Skp2 residues to promote interaction with MO25 and subsequent activation of the protein[68]. Finally, farnesylation of STK11/LKB1 has been reported at C433 at the C-terminal of the protein and affects protein localization at the plasma membrane to regulate mesenchymal polarization by localizing STK11/LKB1 at the leading edge of motile cells[69,70].

1.9.2 Downstream substrates of STK11/LKB1

AMPK

AMPK is recognized as a master regulator of cellular energy metabolism and the best characterized target of STK11/LKB1. When the AMP/ATP ratio changes due to increase in AMP levels or decrease in ATP levels, AMP induces an allosteric change in the AMPK protein allowing T172 to be phosphorylated by STK11/LKB1[71-73]. Activation of AMPK leads to a variety of downstream molecular consequences including fatty acid intake,

autophagy, inhibition of fatty acid synthesis and downregulation of mTORC1 activity. This results generally in a decrease of cell growth and proliferation. Initial studies in budding yeast pointed to kinases Elm1, Pak1 and Tos3 which displayed similarity to STK11/LKB1 as capable to phosphorylate Snf1, yeast homolog of mammalian AMPK[74-76]. These studies were followed by investigation of STK11/LKB1 in mammalian systems where this kinase was able to phosphorylate AMPK *in-vitro* T172 with 100-fold increase in kinase activity if STK11/LKB1 was present with STRAD and MO25 in a heterotrimeric complex. Furthermore, cell lines lacking STK11/LKB1 expression such as HeLa are unable to activate AMPK even in the presence of cellular stress or the pharmacological agonists phenformin or 5-aminioimidazole-4-carboxamide ribo-side (AICAR)[71-73]. Despite being recognized as the main target of LKB1, AMPK can be phosphorylated at T172 by another 2 kinases, TAK1 and CaMKK2, providing alternative routes for AMPK activation[77,78].

MARKs

Microtubule affinity-regulating kinase 1-4 (MARK1, MARK2, MARK3, MARK4) have important roles in regulation of cell polarity. Initial studies on the homolog of STK11/LKB1 in *C. elegans* Par-4 showed its requirement for establishing cell polarity during early embryogenesis[79]. In addition the Par-1 kinase controls *C. elegans* zygote partitioning and in humans MARKs are Par-1 like isoforms that are phosphorylated *in-vitro* by STK11/LKB1 further suggesting their involvement in cell polarity[80]. More recent work has linked LKB1-MARK signaling axis to the Hippo pathway through regulation of yes-associated protein 1 (YAP), a transcriptional regulator implicated in cell polarity, organ size control and stem

cell activity as well as in tumorigenesis where activation of YAP or loss of its upstream negative regulators cause overgrowth and tumor development in epithelial tissues[81].

BRSKs

Brain-specific kinase 1 and 2 (BRSK1 and BRSK2) are mainly expressed in the brain and at lower levels in testis[82]. Their function is therefore mainly related to brain development. Mutants of *C. Elegans* ortholog sad-1 regulates synaptic vesicle distribution and development of normal synapses[83] while knockout of BRSK1 and BRSK2 in mice causes early neonatal lethality due to defects in neuronal polarity. Embryos from these mice show smaller cortices and neurons lacking distinct axonal and dendritic processes[82]. At the molecular level, BRSK1-2 are phosphorylated primarily by STK11/LKB1 and their activity is independent from AMPK activation or kinase activity of CaMKK[84].

NUAKs

NUAK family members NUAK1 and NUAK2 are proteins expressed in a variety of tissues including heart, kidney, brain, liver and skeletal muscle[85]. They are phosphorylated by STK11/LKB1 in their ubiquitin-associated domain which is localized next to the C-terminal of their catalytic domain[86]. NUAK proteins are involved in control of insulin signaling and glucose uptake. NUAK1 is activated upon stimulation by insulin or insulin-like growth factor 1 (IGF-1)[87,88]. In rat skeletal muscle, phosphorylation of NUAK1 is increased upon AICAR stimulation, indicating a role for AMPK in regulating NUAK1 activity[89]. In cancer, NUAK1 is important for tumor cell survival upon nutrient starvation through suppression of

apoptosis caused by glucose starvation. Moreover, AKT has been shown to phosphorylate NUAK1 which in turn regulates apoptosis and cancer cell invasiveness[87,88].

SIKs

Salt inducible kinases (SIKs) are a family of proteins comprised of 3 isoforms: SIK1, SIK2 and SIK3. Initial studies identified SIK in adrenal cortex of rats on an high-salt diet and therefore its expression is particularly abundant in the adrenal cortex where it is an important regulator of hormonal stimulation[90]. SIKs are considered metabolic transmitters in both physiological conditions and cancer. SIK2 promotes insulin resistance and diabetes by gluconeogenesis inhibition in muscles and white adipose tissues[91], while in cancer cell lines its function primarily affects resistance to insults such as nutrient deprivation and taxol chemotherapy[92]. Moreover, domain-focused CRISPR screens revealed high dependency on SIK3 and STK11/LKB1 as its upstream regulator in AML cancer cell lines. Histone Deacetylase HDAC4 was identified as a key SIK3 phosphorylation substrate and its activity was diminished upon targeting of either STK11/LKB1 or SIK3 leading to repression of the oncogenic lineage-specific transcription factor MEF2C[93].

SNRK

SNF Related Kinase (SNRK) is involved mainly in maintaining homeostasis in the cardiac system, the adipose system and in inflammation. Specifically, knockout of *Snrk* in mice results in neonatal lethality with enlarged hearts due to defects associated with cardiac tissue energy sources such as lipids and glycogen[94]. SNRK is expressed in white and brown

adipocytes and its suggested function is to activate insulin-stimulated AKT phosphorylation and glucose uptake in adipocytes[95]. In inflammation, SNRK is believed to suppress NF-Kb signaling and decrease inflammation associated with fibrosis in cardiac and renal tissues[96]. As a consequence, knockout of SNRK in cardiomyocytes increases phosphorylation of NF-kb P65 leading to increased production of pro-inflammatory cytokines, while microRNA 103a-3p suppresses SNRK expression in glomerular endothelial cells leading to renal inflammation and fibrosis[97].

1.9.3 STK11/LKB1 in Peutz-Jeghers syndrome

Peutz-Jeghers syndrome (PJS) is an autosomal dominant disease characterized by the development of benign polyps in the gastrointestinal tract, abnormal melanin pigmentation and increased susceptibility to malignant cancer. Patients with PJS frequently develop small bowel obstruction that is treated by surgical interventions[98]. Mortality in PJS is related to the development of malignant neoplasia. The risk for PJS patients to develop any first cancer by ages 20 to 70 were 2% to 85%, indicating increasing risk with age and a 4-fold increase in risk compared to the general population. The most common cancers observed in PJS patients are colorectal cancer, breast cancer and pancreatic cancer[99,100].

Two independent groups in 1998 discovered that inactivation of the *STK11* gene is the cause of PJS[101,102] , while more recent studies found that 66 to 94% of PJS cases have a germline mutation in *STK11*[103]. Interestingly, no mutations have been found in STK11 interacting proteins highlighting the importance of STK11/LKB1 in the development of the disease[103].

Gastrointestinal (GI) polyps in PJS have a significant stromal component composed of alpha smooth muscle actin and anti-desmin positive cells within the polyps[104]. PJS has been modeled in mice by inactivating one allele of *Stk11*. These mice display GI polyps that are indistinguishable from polyps arising in the human disease but have the tendency of localizing in the stomach rather than the small intestine[105]. Furthermore, mesenchymal cell targeted inactivation of *Stk11* in mice phenocopies development of GI polyps observed in *Stk11* germline haploinsufficient mice and epithelial proliferation observed in the polyps has been linked to decreased transforming growth factor β (TGFβ) signaling which is critical in the control of epithelial growth[106]. Bi-allelic loss of *Stk11* is not required for the formation of polyps indicating that STK11/LKB1 acts as an haploinsufficient tumor suppressor[106].

1.9.4 STK11/LKB1 in cancer

Lung cancer

Lung cancer is the leading cause of cancer deaths worldwide. Lung cancer development is tightly linked with cigarette smoking patterns, which are the major risk factor for its incidence and mortality[107]. The most common driver mutations observed in lung cancer are epidermal growth factor receptor (EGFR) and KRAS activating mutations. While EGFR mutations are more commonly associated with non-smokers, KRAS mutations occur instead mainly in the smoking population and is associated with a worse prognosis[107]. Somatic mutations of *STK11* are one of the most common co-occurring mutations in lung cancer, with frequency related to smoking status up to 34%[108]. Mouse models of lung cancer with conditional *Stk11* deletion in combination with *Kras*^{G12D} knock-in mutation cause higher

frequency of metastatic lung cancer and squamous cell carcinomas (SCCs), which normally do not develop in the *Kras*^{G12D} background, highlighting the role of STK11/LKB1 as a tumor suppressor in disease progression[109]. Furthermore, *Stk11* deletion in *Kras*^{G12D} mouse models promotes a transdifferentiation of adenocarcinomas to SCCs through upregulation of reactive oxygen species (ROS) and this metabolic adaptation conferred SCCs resistance to phenformin treatment[110].

Cancers of the reproductive tract

Sporadic cervical cancer is tightly associated with human papilloma virus (HPV) infection. HPV infection causes epithelial dysplasia that do not evolve into invasive cancer in the absence of additional genetic lesions[111]. Biallelic inactivating mutations in *STK11* are present in cervical cancer patients and are associated with significantly reduced survival compared with cervical cancer patients with wild type *STK11*. Interestingly, commonly used cervical cancer cell lines, including HeLa, have biallelic *STK11* mutations which correlate with the aggressive characteristics of the cell lines both *in-vitro* and *in-vivo*[111].

Mice with germline haploinsufficiency of *Stk11* also develop frequent uterine endometrial adenocarcinomas, and conditional deletion of *Stk11* by Adeno-Cre virus in the uterine epithelium results in similar lesions with decreased AMPK activity but no evident activation of the mTOR pathway[112]. A further development in modeling uterine adenocarcinoma in mice was achieved with using Sprr2f-Cre mice, which allow specific genetic deletions in epithelial cells of the uterine lumen and endometrial glands. These mice present with

invasive endometrial adenocarcinomas with significant mTOR activation and consequent sensitivity to rapamycin which slowed the progression of *Stk11* deficient tumors[113].

Pancreatic Cancer

A small proportion of pancreatic tumors have been reported to harbor somatic *STK11* mutations and decreased STK11/LKB1 protein expression by immunohistochemistry in pancreatobiliary neoplasms[114]. Most pancreatic tumors arise from constitutive *KRAS* oncogene activation, but mice expressing *Kras*^{G12D} specifically in pancreatic progenitor cells through *Pdx1*-Cre only develop early lesions that rarely progress into invasive pancreatic cancer[115]. When *Kras*^{G12D} mice are combined with conditional knockout of *Stk11* there is a dramatic acceleration of tumorigenesis with mice developing malignant invasive pancreatic ductal adenocarcinomas (PDACs) with reduced expression of p21 and p53. Moreover, 19% of human PDACs expressed low levels of STK11/LKB1 protein by immunohistochemistry and this expression status correlated with lower survival when compared to normal STK11/LKB1 expression[116].

While STK11/LKB1 has been extensively studied in solid malignancies, its role in blood cancer is largely undefined. Of note, three reports have described the essential role of STK11/LKB1 in normal hematopoiesis. In mouse models, hematopoietic specific loss of STK11/LKB1 causes a bone marrow failure phenotype associated with exhaustion of HSCs[117-119]. In an effort to uncover potential tumor suppressors involved in the progression

of MPNs to MPN-BP, we performed an unbiased CRISPR screen in mouse MPN cells which revealed a role for STK11/LKB1 in the leukemic progression of MPNs.

CHAPTER II

EVALUATION OF THE AURORA KINASE A INHIBITOR ALISERTIB IN THE TREATMENT OF HUMAN PRIMARY MYELOFIBROSIS

Studies underlining the importance of the megakaryocyte lineage in PMF encouraged further investigations to therapeutically target these cells. An initial effort by the Crispino lab identified small molecules dimethylfasudil (diMF) and MLN8237 (Alisertib) to be capable of increasing polyploidization of acute megakaryoblastic leukemia (AMKL) cell lines. These small molecules were shown to inhibit Aurora Kinase A (AURKA) and displayed potent anti-AMKL activity *in-vivo*[38]. Moreover, given the link between megakaryocyte expansion and bone marrow fibrosis, Alisertib was tested in preclinical models of PMF. Treatment of *MPL*^{W515L} mice and *Jak2*^{V617F} knock-in mice with Alisertib lead to decreased disease burden, reduction of megakaryocyte hyperplasia and significant reduction in bone marrow fibrosis[120].

Given the encouraging results in preclinical models, a Phase I clinical trial for the treatment of PMF with Alisertib was opened to evaluate the safety and efficacy of the drug and perform correlative studies to verify on-target effects on the megakaryocyte lineage.

2.1 Baseline characteristics of patients and treatment regimen

A phase I open label clinical trial was led by Dr. Stein at Northwestern University with additional investigators including Dr. Gangat and Dr. Tefferi at the Mayo Clinic and Dr. Swords at the University of Miami. Seventeen patients with primary myelofibrosis, four with post-thrombocythemia myelofibrosis and 3 with post-polycythemia vera myelofibrosis were enrolled in the clinical trial for a total of 24 patients. The median age of the patients was 72 years with 67% males. According to the Dynamic International Prognostic Scoring System

(DIPSS), 33% of the patients were DIPSS intermediate-1 risk, 46% were intermediate-2 risk and the remaining were high risk. Fifteen patients had prior exposure to the JAK2 inhibitor Ruxolitinib: 9 of those experienced disease progression, 2 were intolerant and the rest did not respond to the treatment. Nine patients (37%) were JAK inhibitor naïve due to transfusion dependent anemia, absence of splenomegaly and physician preference in a patient with high-risk genotype. Fourteen patients were positive for driver mutations in *JAK2*, seven patients harbored mutations in CALR and 3 patients harbored mutations in MPL. In addition to driver mutations, 10 of 15 patients evaluated presented with one or more high molecular risk mutations. At study entry 58% of patients showed a palpable splenomegaly ≥ 5 cm below the left costal margin and 54% were red cell transfusion dependent. Additional clinical characteristics are showed in Table 1.

Patients received a median of 7.5 cycles of therapy (range: 1-29 cycles). Reasons for treatment discontinuation included progressive disease in five patients, lack of response in eleven patients after a median of 7 cycles, toxicity in four patients after a median of 7 cycles and refusal of further therapy in 2 patients. 2 patients transformed to acute myeloid leukemia with survival of 3 and 6 months, respectively.

Characteristics	All patients ($n = 24$)
Median age (range)	72 (48–80)
Male, *n* (%)	16 (67)
Female, *n* (%)	8 (33)
Race, *n* (%)	
Caucasian	22 (92)
Other	2 (8)
Myelofibrosis classification, *n* (%)	
Primary	17 (71)
Post-thrombocythemia/myelofibrosis	4 (17)
Post-polycythemia vera/myelofibrosis	3 (13)
DIPSS risk classification, *n* (%)	
Intermediate-1	8 (33)
Intermediate-2	11 (46)
High	5 (21)
Median MPN-SAF score (range)	31 (2–70)
Palpable splenomegaly, *n* (%)	14 (58)
Transfusion dependence	13 (54)
Median disease duration in years (range)	2.8 (0.08–35.5)
Median white blood cells (range; $\times 10^9$)	7.45 (1.50–91.00)
Median hemoglobin (range; g/dL)	9.45 (6.10–14.80)
Median platelets (range; $\times 10^9$)	177 (74–1,431)
Prior use of JAK inhibitor, *n* (%)	15 (63)
Mutation type, *n* (%)	
JAK2	14 (58)
CALR	7 (29)
MPL	3 (13)

Table 1 - Baseline patient characteristics

2.2 Alisertib has on-target effects on human PMF megakaryocytes

In preclinical models of myelofibrosis, Alisertib was shown to target mutant mouse megakaryocytes and reduce bone marrow fibrosis[120]. To evaluate if Alisertib has on target effects on human megakaryopoiesis, we isolated human CD34+ progenitors from peripheral blood of PMF patients enrolled in the trial before the beginning of treatment, expanded them

in vitro for 5 days and then induce megakaryocyte differentiation with thrombopoietin in the presence of Alisertib or Ruxolitinib and then assessed megakaryocyte differentiation and apoptosis in the CD41+CD42+ compartment by DNA content analysis and Annexin V staining using flow cytometry (Fig 1A). Alisertib strongly induced polyploidization and apoptosis in a dose-dependent manner in all five specimens tested. By contrast, Ruxolitinib showed little response in the polyploidization and apoptosis of mutant CD41+CD42+ megakaryocytes (Fig 1B). Importantly, 3 of these patients (05-01-18, 05-01-14 and 01-20) failed prior JAK inhibitor therapy. These results show that Alisertib has on target effects on the megakaryocytic lineage inducing differentiation by polyploidization and subsequent apoptosis of mutant megakaryocytes.

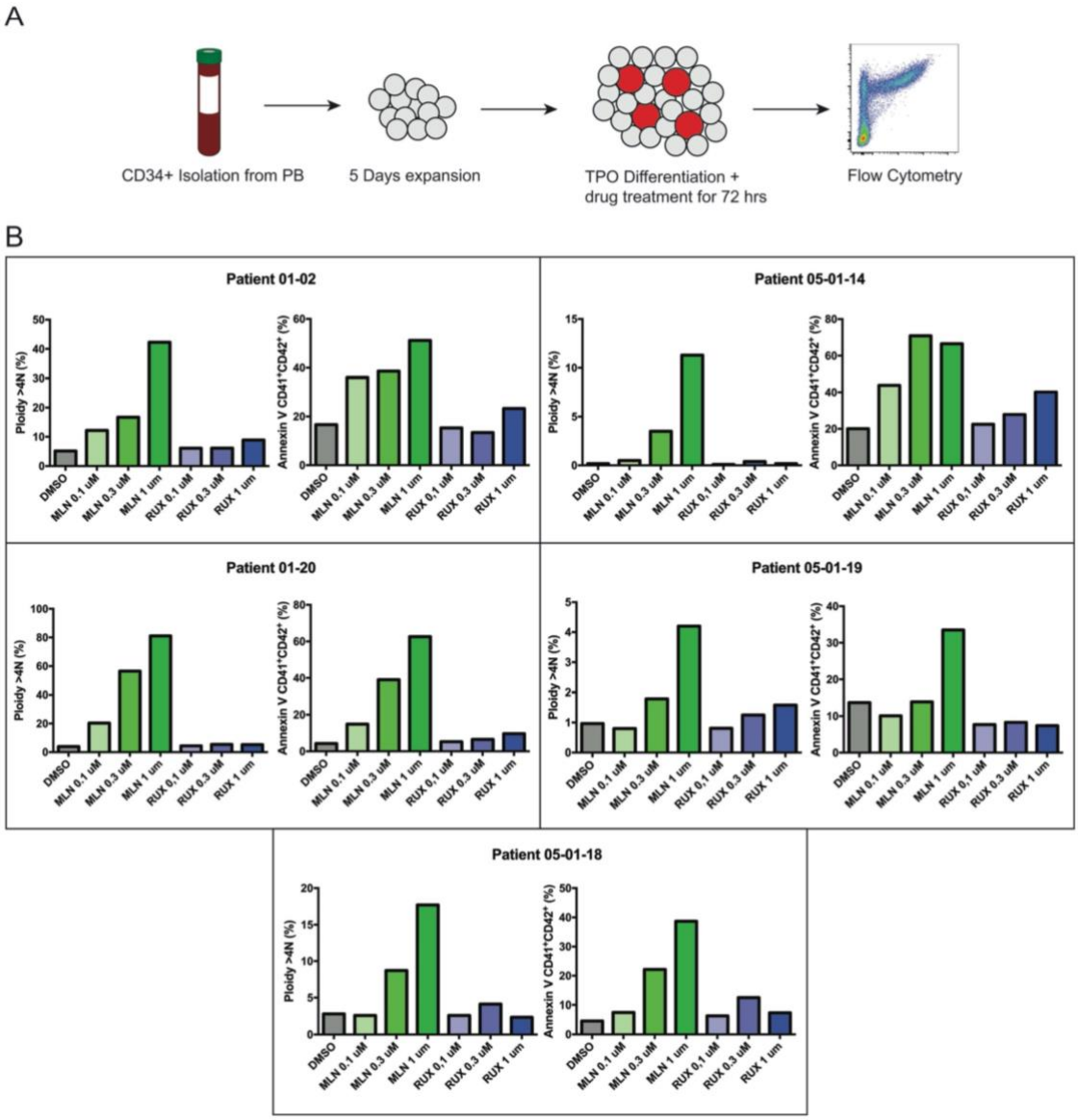

Figure 3 - Alisertib but not Ruxolitinib enhanced polyploidization and apoptosis of patient-derived mutant megakaryocytes *ex vivo*. A. Experiment schematics **B.** Polyploidization and apoptosis of patient-derived CD41+CD42+ mutant megakaryocytes in presence of increased doses of Alisertib versus Ruxolitinib. Data for 5 individual patients are shown.

2.3 Alisertib does not consistently affect cytokine levels

One of the effects of JAK inhibition in patients is the ability to induce a rapid reduction in inflammatory cytokines which in turn results in reduction of splenomegaly[16].

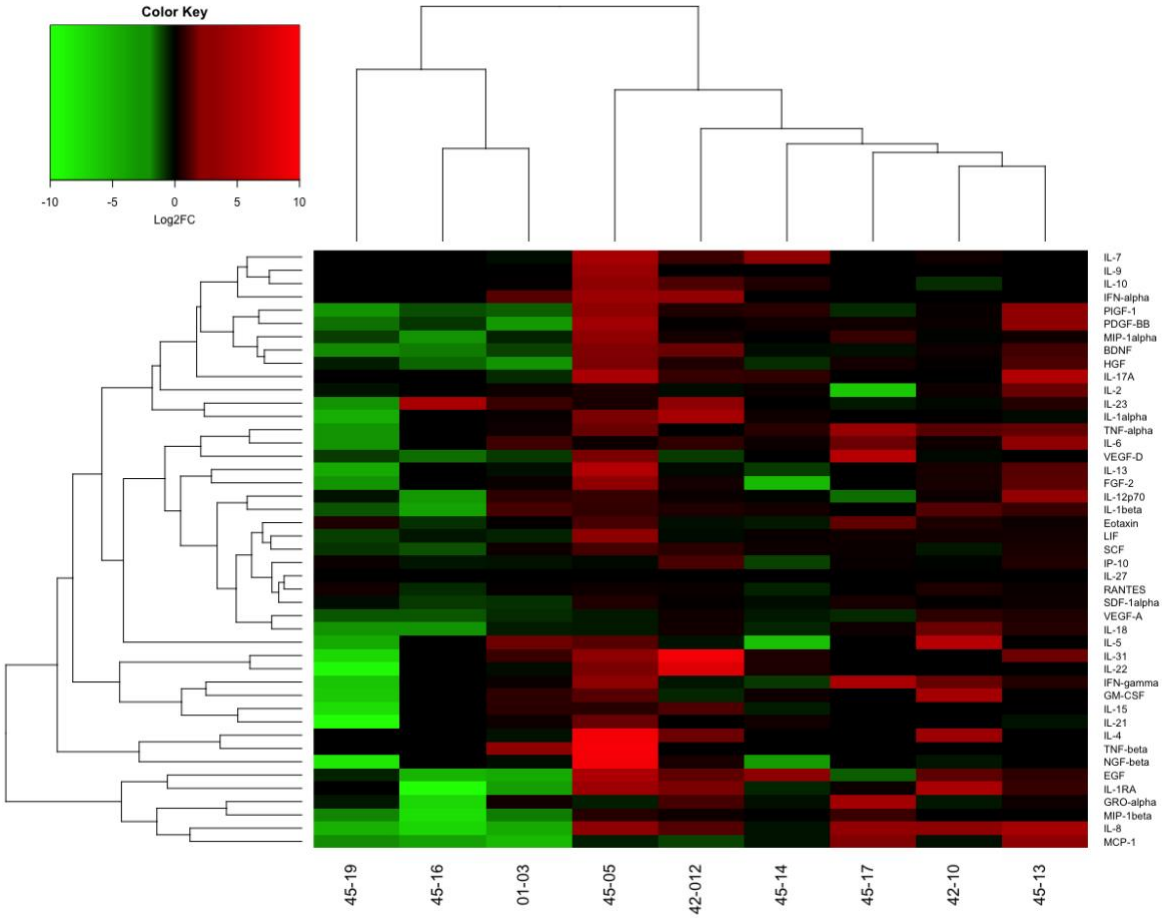

Figure 4 - Heatmap showing Log2 fold change at cycle 5 relative to baseline of 45 cytokines in serum samples and separated based on unsupervised clustering.

To determine whether AURKA inhibition by Alisertib cause a similar response, we performed Luminex Cytokine profiling and an ELISA assay for TGF-β on peripheral blood serum samples from 9 paired alisertib-treated patients pre- and post-treatment. We failed to

see a consistent response, with two patients showing an overall decline in the inflammatory cytokines, 3 with mixed responses and 4 that showed an overall increase in cytokines levels (Fig 2). TGF-β is a cytokine excessively produced by mutant MPN megakaryocytes and it is believed to support bone marrow fibrosis in PMF. We did not see increased levels of TGF-β post-treatment, and there were several patients showing as much as 50% reduction in TGF-β (Fig 3). These observations suggest that Alisertib reduces spleen size through a mechanism different from Ruxolitinib.

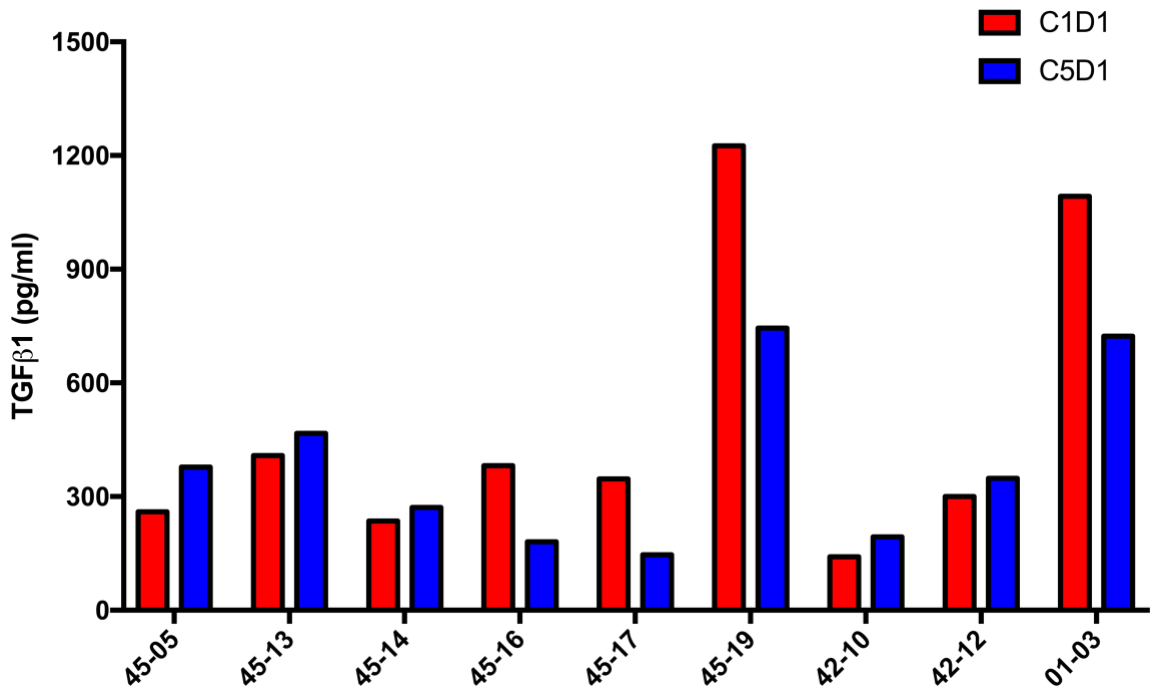

Figure 5 - Bar graph showing levels of TGF-β1 in the serum of 9 patients at C1D1 (pre-treatment) and C5D1 (post-treatment).

2.4 Alisertib normalizes megakaryocyte morphology, decreases fibrosis and rescues GATA1 levels in human PMF

Atypical megakaryocytes in the bone marrow of MPN patients and animal models with *JAK2*, *CALR*, or *MPL* mutations fail to stain for GATA1[34]. To investigate whether alisertib, as part of its ability to promote megakaryocyte maturation and polyploidization, could up-regulate GATA1 protein levels, we treated the SET2 post-MPN AML cell line with alisertib. By intracellular flow cytometry, we observed robust increase in GATA1 expression in parallel with a marked increase in the ploidy state (Fig 4A,B)

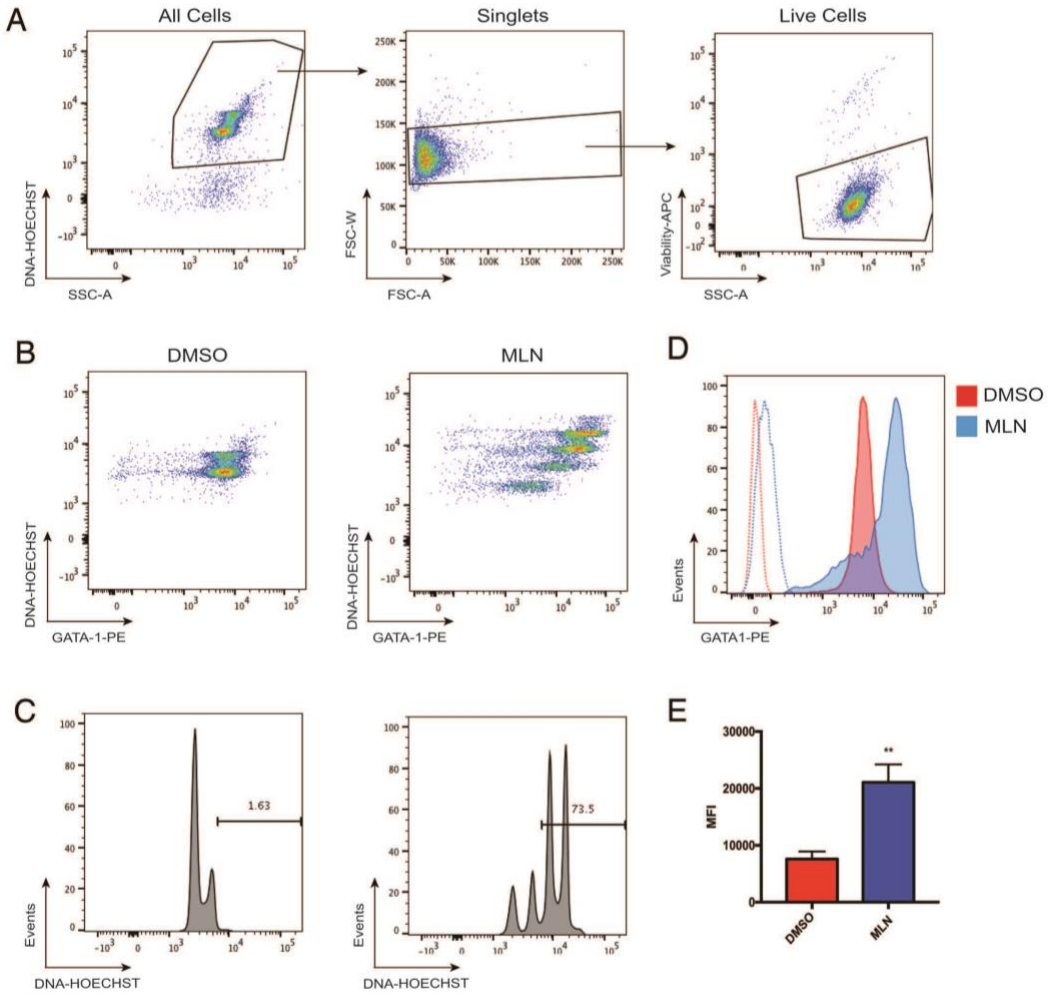

Figure 6 - Alisertib induced GATA1 expression in the SET2 megakaryocytic cell line. A) Gating strategy. B, C) Representative flow cytometry data of DNA content following 72 hours of culture with DMSO or 1 μM alisertib (MLN). D,E) Representative flow cytometry data (D) and mean fluorescence intensity (MFI) measurements (E) for three independent experiments following intracellular staining for GATA1. Means +/- standard error are shown. ** $p<0.01$.

To assess the effect of Alisertib on human hematopoiesis in PMF patients, we obtained bone marrow biopsies from 7 patients at baseline and after a minimum of 5 cycles of therapy. H&E staining revealed an improvement of megakaryocyte morphology in 6 out of 7 patients (86%), with restoration of multilobed nuclei and absence of clustering which is normally seen in PMF patients as a result of expansion of the megakaryocyte lineage (Fig 5A,B). We recently reported that impaired megakaryopoiesis in human PMF is caused by reduced expression of the hematopoietic transcription factor GATA1. Atypical megakaryocytes from both animal models with JAK2, CALR or MPL mutations and human MPN fail to stain for GATA1. Immunohistochemistry (IHC) for GATA1 revealed a striking increase of staining in 6 out of 7 patients (86%). GATA1-positive cells included both erythroid cells and megakaryocytes with an increased proportion of GATA1-positive megakaryocytes in all cases (Fig 5A,B, Table 2). The 1 patient that did not show a GATA1 improvement entered the study as a patient with post-AML myelofibrosis and who progressed to AML after 1 year of therapy.

In addition to restoration of morphology and GATA1 levels, we observed reduction of bone marrow fibrosis in 5 out of 7 cases (71%), with one of the non-responders being the one who progressed to AML (Fig 5A,B, Table 2). The reduction in fibrosis was accompanied by sustained responses to the drug. For example, For example, patients 42-01, 01-03, and 42-10 maintained a symptom and spleen response for more than 12 weeks, whereas 01-02 and 05-01-09 exhibited a symptom and anemia response or a symptom response for more than 12 weeks, respectively.

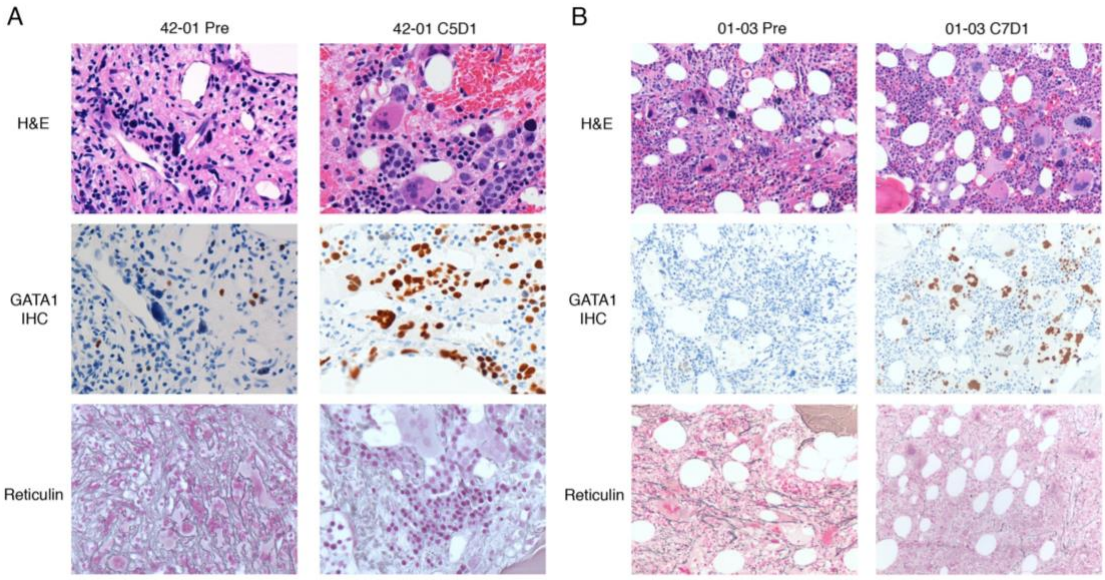

Figure 7 - Alisertib restored GATA1 staining to megakaryocytes and reduced bone marrow fibrosis. Images of bone marrow biopsies stained with H&E, an anti-GATA1 antibody, or for reticulin from patients 42-01 (**A**) and 01-03 (**B**) pre- and during therapy. Original magnification, 400X.

Patient	Cycle	GATA1 staining	Fibrosis grade	Best Response
42-01	Pre C5D1	24% positive 68% positive	MF3 MF2	Spleen and symptom (not anemic)
01-02	Pre C6D17 EOS	60% positive 28% positive Weak Staining	MF3 MF3 MF3	Symptom and anemia (spleen not palpable)
01-03	Pre C7D1	35% positive 73% positive	MF3 MF2	Spleen and symptom (not anemic)
05-01-05	Pre C17D1	25% positive 69% positive	MF3 MF2	Stable disease
05-01-09	Pre C19D1	70% positive 95% positive	MF3 MF2	Symptom (spleen not palpable, not anemic)
42-10	Pre C7D15	50% positive 70% positive	MF3 MF3	Spleen and symptom (not anemic)
05-01-13	Pre C11D1	61% positive 88% positive	MF2 MF1	Stable disease

Table 2 - Association between GATA1 staining, degree of fibrosis and clinical response

In summary, this Phase I clinical trial showed that Alisertib was overall well tolerated and has activity in PMF patients. Alisertib has on target effects on the megakaryocytic lineage and this effect leads to normalization of megakaryocyte morphology, increased GATA1 staining and decrease of bone marrow fibrosis.

2.5 Discussion

Although we developed megakaryocytic polyploidization agents initially to target malignant megakaryocytes in Acute Megakaryoblastic Leukemia, we discovered that these compounds also induced maturation of the atypical megakaryocytes that characterize myelofibrosis[120]. Our preclinical studies revealed that AURKA inhibition potently induced polyploidization,

features of maturation, and subsequent apoptosis of megakaryocytes from MPN mouse models and patient samples[121]. Our studies also showed that alisertib suppressed the myeloproliferative and fibrotic phenotypes caused by expression of activated alleles of *JAK2* or *MPL* in animal models of the MPNs.

In concert with the phase 1 study of alisertib in the MPNs, we evaluated the activity of alisertib in a number of correlative studies. Of note, we found that alisertib improved the morphology and GATA1 staining of the megakaryocyte lineage. Furthermore, unlike Ruxolitinib, alisertib therapy was not associated with consistent changes in peripheral blood cytokines, including TGF-β, which has been implicated in driving bone marrow fibrosis. These results indicate that alisertib is not acting as an anti-inflammatory but rather through a novel mechanism targeting megakaryocytes and possibly other lineages as well. Moreover, the finding that patient 01-02 showed clinical improvement despite the lack of improved GATA1 staining suggests that alisertib has antitumor properties that are independent of the megakaryocyte differentiation effect. This effect of alisertib on other cells begs the question of whether the reduction in fibrosis is only due to normalization of megakaryocytes. We cannot exclude the possibility that alisertib affects other lineages, such as osteoblasts, which have been implicated in driving fibrosis in myeloproliferative disorders[122].

With respect to the mechanism by which alisertib leads to increased GATA1 expression in patients, we envision three scenarios. First, it is possible that AURKA inhibits the activity of megakaryocyte differentiation transcription factors, such as NFE2, by direct phosphorylation and that AURKA inhibition then enables this factor to promote maturation,

which would be expected to be accompanied by increased GATA1 expression. Second, GATA1 expression may be elevated as a consequence of the increased degree of polyploidization, that is, increased transcription concomitant with increased number of *GATA1* alleles. A third possibility is that the increased proportion of GATA1-positive megakaryocytes seen with treatment reflects an increase in nonmalignant hematopoiesis. However, because alisertib increased GATA1 expression in SET2 cells in culture and did not reduce the mutant allele burden in all cases, the former two possibilities are more likely.

The results of this phase I study are significant in a number of respects. First, we demonstrate that alisertib is overall well tolerated in patients with myelofibrosis with prolonged administration up to 1.7 years and also report that alisertib provided clinical benefit to this group of patients, over half of whom were heavily pretreated. These results are important given the limitations of current myelofibrosis therapies, including those of ruxolitinib, which include an average duration of response of 2–3 years. Second, alisertib restored normal morphology and GATA1 expression to the pathognomonic atypical megakaryocytes and further, reduced the degree of bone marrow fibrosis. The effects were generally associated with sustained clinical responses. A notable exception was patient 01-02 whose marrow showed a decline in GATA1 staining and no improvement in fibrosis with treatment. Despite a sustained symptom and anemia response, this patient developed AML after 19 cycles. These data underscore the critical contributions of megakaryocytes to the fibrotic process in myelofibrosis and highlight the unique activity of AURKA inhibition on this lineage. Third, the results also suggest that atypical megakaryocytes are required for the maintenance of

fibrosis. Together, these data provide a strong rationale for the further study of AURKA inhibition as a therapeutic option in myelofibrosis and provide direct evidence that megakaryocytes with activated JAK/STAT signaling promote bone marrow fibrosis in humans.

CHAPTER III

STK11/LKB1 IS A TUMOR SUPPRESSOR IN THE LEUKEMIC TRANSFORMATION OF THE MYELOPROLIFERATIVE NEOPLASMS

3.1 A focused CRISPR/Cas9 screen reveals Stk11 loss as a driver of HSPC self-renewal

To investigate tumor suppressor genes that drive leukemic transformation in cells with activated JAK/STAT signaling, we performed a positive CRISPR/Cas9 screen by transducing two curated lentiviral single-guide RNA (sgRNA) libraries, each containing four sgRNAs targeting ~100 unique annotated tumor suppressors and several MPN associated genes as well as 50 non-targeting control sgRNAs, in *Jak2*^{V617F} c-kit^{+} HSPCs constitutively expressing Cas9 from the Rosa26 locus and assessed their serial replating capacity in methylcellulose media (Fig 7A). *Trp53* was intentionally omitted from both libraries due to previous reports already identifying it as a transformation factor for *JAK2* mutant MPNs.

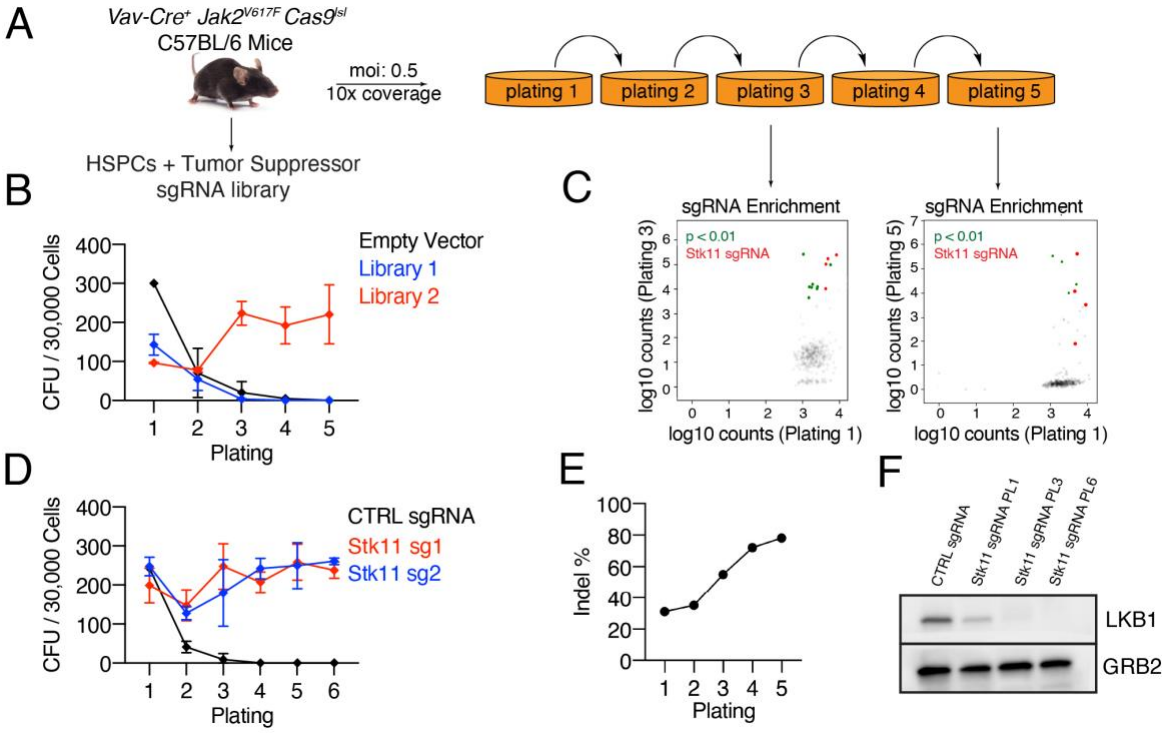

Figure 8 - CRISPR/Cas9 screening reveals loss of LKB1 is a driver of serial re-plating of *Jak2*^{V617F} hematopoietic cells. A) Schematic of the experimental workflow. B) Number

of hematopoietic colonies formed at each generation of plating for *Jak2*^{V617}/Cas9/Vav-Cre cells infected with library 1 or 2. The average of 2 biological replicates plus/minus SD are shown. C) sgRNA enrichment of plating 1 versus 3 or 5 as determined by DNA sequencing. sgRNAs targeting *Stk11* are highlighted in red. The P value represents significance by Fisher's exact test. D) Number of hematopoietic colonies formed over 6 generations for *Jak2*^{V617F}/Vav-Cre cells targeted with two independent sgRNA targeting *Stk11*. The average plus/minus SEM are shown, n=3. E) ICE analysis of the extent of *Stk11* targeting in cells from (B). F) Western blot for LKB1 levels at the various stages of re-plating of *Jak2*^{V617F} cells electroporated with RNPs against *Stk11*. GRB2 is displayed as the loading control.

Transduction of either library 1 or 2 in Vav-Cre/Cas9^{lsl} lin^{-} HSPCs did not result in enhanced replating (Fig S1A), while CRISPR editing of *Trp53* in *Jak2*^{V617F} c-kit^{+} HSPCs as a positive control resulted in enhanced serial replating as expected (Fig S1B, C). By contrast, transduction of library 2 led to robust serial replating of *JAK2*^{V617F} cells over 5 generations while transduction of library 1 or a control empty vector failed to induce this phenotype (Fig 7B). Next generation sequencing (NGS) of DNA obtained from cells at plating 1 as a baseline versus plating 3 showed enrichment of all four guides present in the library that target Serine/Threonine Kinase 11 (*Stk11*), which encodes LKB1 (Fig 7C), while two sgRNAs targeting *Stk11* were significantly enriched at plating 5. To confirm the *Stk11* result of the screen, we electroporated ribonucleotide complexes (RNPs) containing Cas9 and two independent sgRNAs targeting *Stk11* in *Jak2*^{V617F} c-kit^{+} HSPCs and performed a serial replating assay. Cells electroporated with either *Stk11* sgRNA induced a strong serial

replating over 6 generations while cells electroporated with the control sgRNA failed to replate (Fig 7D). To evaluate the efficiency of sgRNA targeting, we sequenced a region of *Stk11* flanking the Cas9 cut site and performed Inference of CRISPR Edits (ICE) analysis on the resulting chromatograms from Sanger sequencing. The percentage of productive indels increased from plating 1 to plating 5 indicating progressive enrichment of *Stk11* knockout cells during replating (Fig 7E). Finally, we performed western blot analysis for LKB1 levels in cells at different stages and observed strong down-regulation of LKB1 expression (Fig 7F). Together, these results show that loss of the tumor suppressor *Stk11* is a driver of *in-vitro* self-renewal in *Jak2*^{V617F} MPN cells.

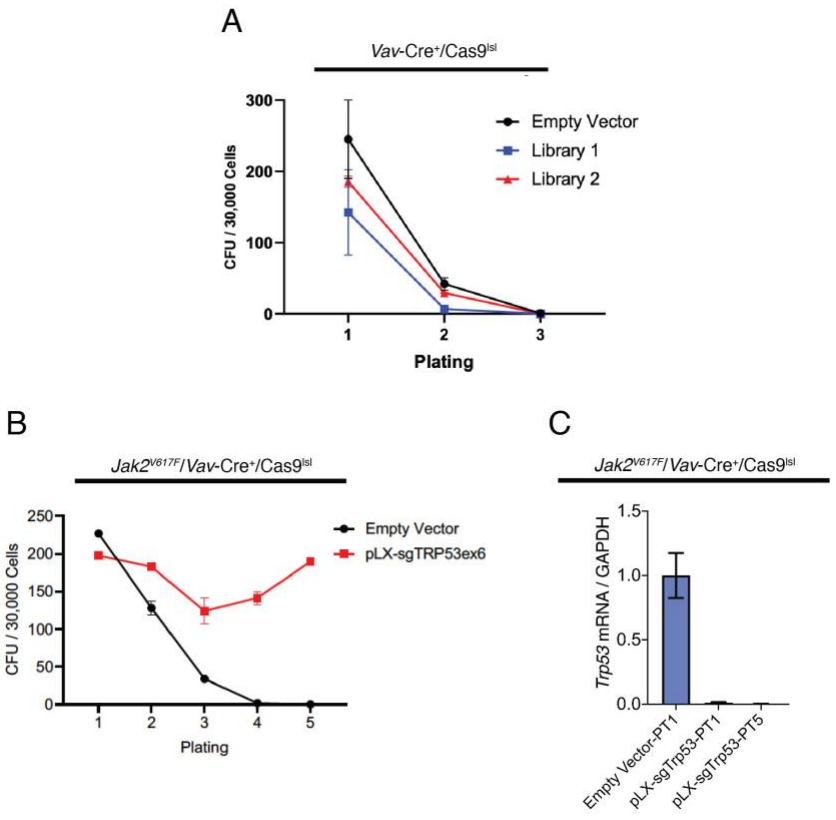

Supplemental Figure 1: Negative and positive controls of the CRISPR screen. A) Serial replating colony forming unit assays of *Vav*-Cre/Cas9^{lsl} cells transduced with Library 1,

Library 2 or empty vector as a control. The average +/- SEM are shown, n=2 biological replicates. B) Serial replating colony forming unit assays of *Jak2*^{V617F}/*Vav*-Cre/Cas9^{lsl} c-kit^{+} hematopoietic progenitor cells transduced with a vector encoding a sgRNA targeting exon 6 of *Trp53* or empty vector. Data depict the average +/- SEM for 2 biological replicates. C) qRT-PCR data showing the decrease in *Trp53* mRNA upon gene editing. The averages +/- SEM of 2 biological replicates are shown.

3.2 LKB1 loss in MPN cells induces transcriptional changes related to hypoxia, oxidative phosphorylation and the stem cell program

Hematopoietic specific depletion of *Stk11* in mice leads to bone marrow failure due to an initial burst of proliferation of *Stk11*-deficient HSCs followed by their depletion[119]. To confirm the phenotype induced by *Stk11* loss with a different MPN driver mutation, we obtained *Stk11*$^{fl/fl}$ mice. We co-transduced *Stk11*$^{fl/fl}$ c-kit^{+} HSPCs with a retroviral vector encoding the MPN driver mutation *MPL*^{W515L} and an mCherry reporter (Migr1-MPL^{W515L}-mcherry) along with a retroviral vector encoding CRE recombinase and a GFP reporter (Migr1-CRE-GFP) to induce *Stk11* deletion, sorted mCherry-GFP double positive cells and cultured them in methylcellulose media (Fig. 8A). As with the *Jak2*^{V617F} genotype, hematopoietic progenitor cells expressing MPL^{W515L} alone failed to serially replate (Fig 1H). By contrast, homozygous deletion of *Stk11* in combination with *MPL*^{W515L} (*MPL*^{W515L}/*Stk11*$^{\Delta/\Delta}$) led to a robust replating phenotype similar to the *Jak2*^{V617F} /*Stk11* targeted cells while those with empty vector control (CTRL), *Stk11* deletion alone, or *MPL*^{W515L} overexpression alone failed to replate (Fig. 8B). Of note, *MPL*^{W515L} *Stk11*$^{\Delta/\Delta}$ cells

also grew in cytokine free methylcellulose media and in liquid culture in a cytokine independent fashion with an immature morphology when transferred from cytokine free methylcellulose to liquid culture (Figure S2).

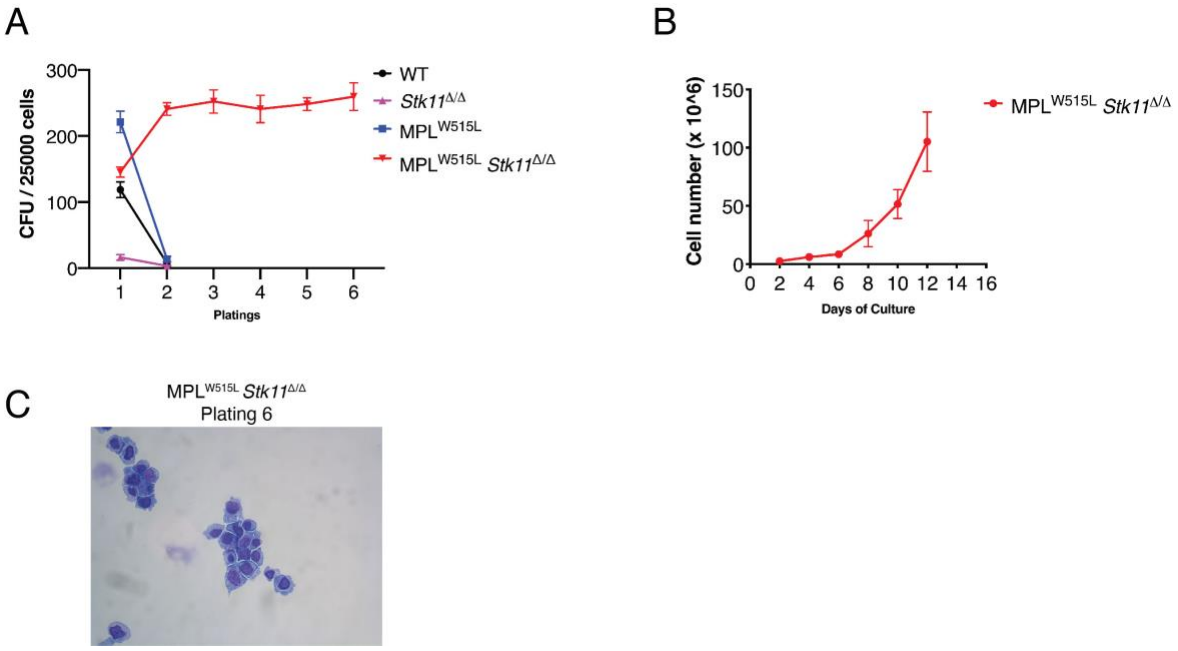

Supplemental Figure 2: Cytokine independent growth of MPL^{W515L}/*Stk11* $^{\Delta/\Delta}$ cells. A) Serial replating colony forming unit assays of MPL^{W515L}/*Stk11* $^{\Delta/\Delta}$ cells and single controls in cytokine free methylcellulose media. The average plus/minus SD are shown, n=3 biological replicates. B) Growth of MPL^{W515L}/*Stk11* $^{\Delta/\Delta}$ cells in liquid culture over 12 days. The average +/- SD are shown, n=2 biological replicates. C) Giemsa staining of MPL^{W515L}/*Stk1* $^{\Delta/\Delta}$ cells at plating 6.

To investigate the transcriptional changes that characterize the replating phenotype, we performed RNA-seq on CTRL and *MPL*^{W515L} cells at plating 1 along with *MPL*^{W515L}/*Stk11*$^{\Delta/\Delta}$ cells at platings 1, 3 and 6. Multidimensional Scaling (MDS) plot showed a distinct

clustering of *MPL*^{W515L}/*Stk11*$^{\Delta/\Delta}$ from CTRL and *MPL*^{W515L} cells (Fig. 8C). Differential expression analysis across all the conditions resulted in 5463 genes differentially expressed genes, and unsupervised hierarchical clustering of these genes highlighted a transcriptional signature separated from CTRL and *MPL*^{W515L} cells (Fig 8D). To identify genes specifically associated with deletion of *Stk11* in the context of JAK/STAT activation, we performed differential expression analysis on *MPL*^{W515L} *Stk11*$^{\Delta/\Delta}$ cells versus *MPL*^{W515L} cells at plating 1. *Stk11* deletion had a profound effect on the transcriptome of *MPL*^{W515L} cells and resulted in 1527 genes being differentially expressed (Fig. 8E). Gene Set Enrichment Analysis (GSEA) revealed enrichment of pathways related to hypoxia, embryonic stem cells, and regulation of oxidative phosphorylation (OXPHOS) in the *MPL*^{W515L}/*Stk11*$^{\Delta/\Delta}$ phenotype, while pathways related to myeloid differentiation, maturation of hematopoietic cells and interleukin-6 production were enriched in the *MPL*^{W515L} MPN cells (Fig 8F,G, Fig S3). Together, these data demonstrate that loss of *Stk11* results in the same self-renewal phenotype in both *JAK2* and *MPL* mutant settings and induces profound transcriptional changes that separate immature *MPL*^{W515L} *Stk11*$^{\Delta/\Delta}$ cells from the differentiated state of *MPL*^{W515L} MPN cells.

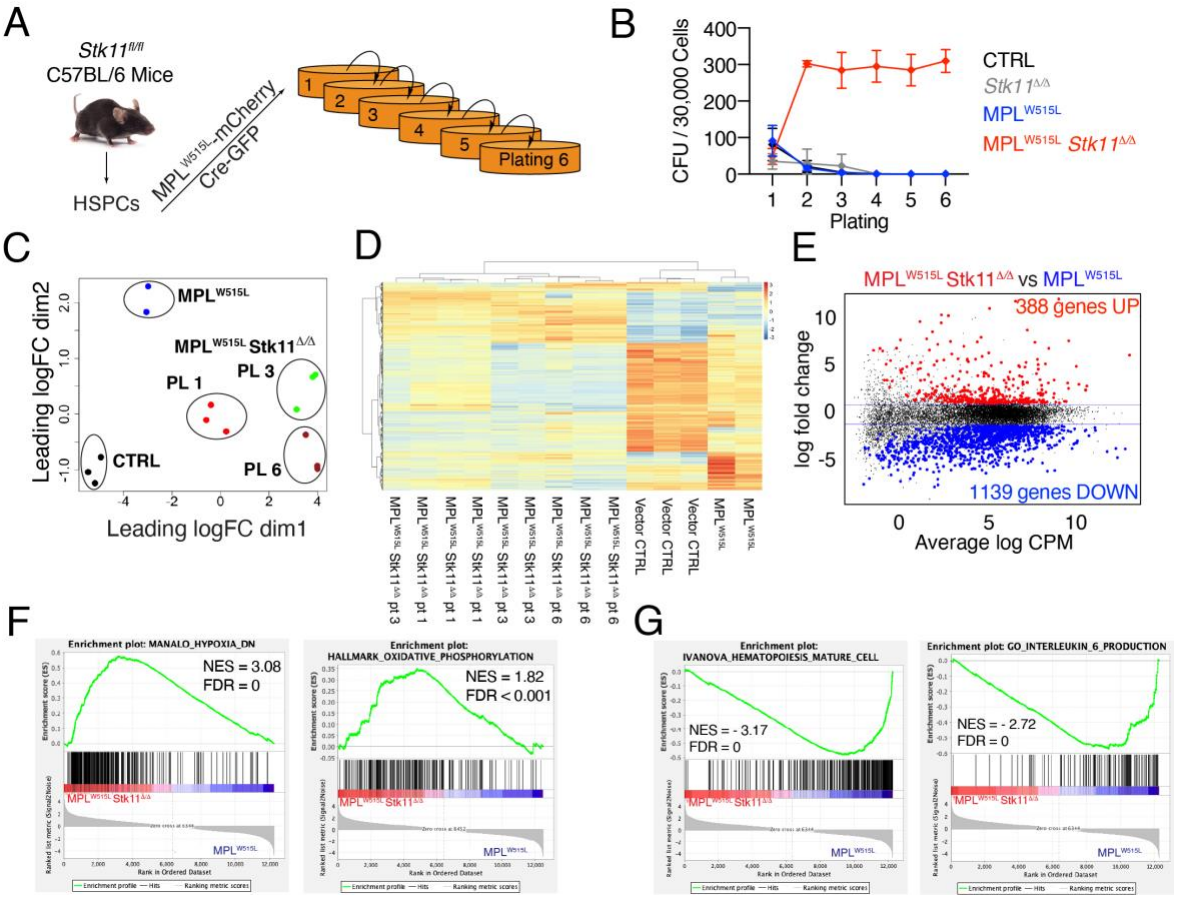

Figure 9 – *Stk11* loss in MPL^{W515L} mutant cells drives serial replating. A) Schematic of the experimental workflow for the MPL^{W515L} studies. B) Number of hematopoietic colonies formed for up to six generations for murine *Stk11*-floxed HSPCs expressing various combinations of MPL^{W515L} and Cre. The average plus/minus SD are shown, n=6 C) MDS plot of RNA-seq data comparing MPL^{W515L}/*Stk11*-null to MPL^{W515L}/*Stk11*$^{+/+}$ cells after one round of plating. D) Unsupervised clustering analysis comparing RNA-seq data from cells collected after the first round of plating for control and MPL^{W515L}/*Stk11*$^{+/+}$ and at first, third and sixth plating for MPL^{W515L}/*Stk11*-null cells. E) MA plot of the comparison MPL^{W515L}/*Stk11*-null versus MPL^{W515L}/*Stk11*$^{+/+}$ at plating one showing differentially

expressed genes. F,G) Pathways that are correlated with the MPL^{W515L}/*Stk11*-null phenotype (F) or correlated with the MPL^{W515L} phenotype (G) by GSEA analysis.

A

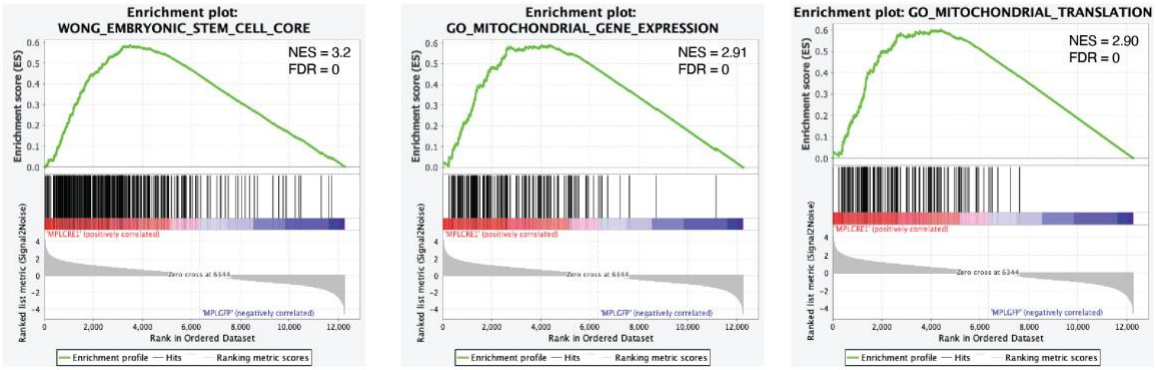

B

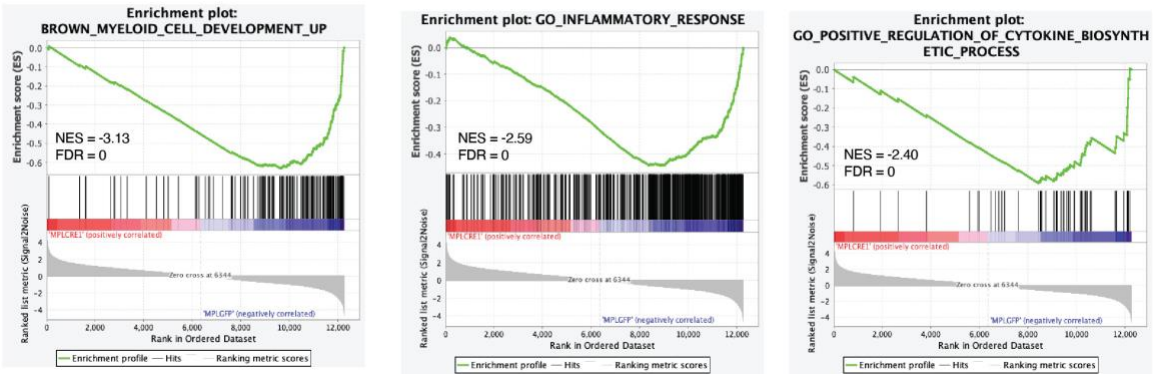

Supplemental Figure 3: Additional pathways that are correlated with the MPL^{W515L}/*Stk11*-null phenotype (A) or correlated with the MPL^{W515L} phenotype (B) by GSEA analysis.

3.3 Enhanced self-renewal of *Stk11*-deficient cells with activated JAK/STAT signaling is associated with HIF1a stabilization

We then investigated the mechanism by which loss of LKB1 contributes to enhanced self-renewal. First, we collected cells from the first-generation methylcellulose cultures of

murine HSPCs of four different genotypes: wild-type (WT), MPL^{W515L}, $Stk11^{\Delta/\Delta}$, and $MPL^{W515L}/Stk11^{\Delta/\Delta}$. Whole cell lysates were then assessed for levels of LKB1 and its well-studied downstream substrate AMPK (Fig 9A). Previous studies have shown that loss of LKB1 did not induce HSC failure through AMPK [117-119], therefore we were not surprised to see that levels of total and p-AMPK at threonine 172 were not substantially depleted by loss of *Stk11*. Of note, overexpression of MPL^{W515L} also did not result in changes in AMPK levels, nor did the combination of *Stk11* loss and MPL^{W515L} expression.

Given the gene expression data which revealed that there was enrichment of the hypoxia geneset by GSEA and substantial upregulation of hexokinase II (HKII), we assessed the expression of these factors in cells of the various genotypes. Consistent with the RNA-seq data, we saw that HKII was markedly upregulated by deletion of *Stk11* and expression of MPL^{W515L} (Fig 9A). In accordance with GSEA, we also observed that HIF1a, the key transcriptional regulator of HKII, was also substantially elevated in the LKB1 deficient cells that expressed MPL^{W515L}. Moreover, stabilization of HIF1a persisted even in cells expanded in liquid culture (Fig S4). These results strongly suggest that activation of JAK/STAT signaling in combination with *Stk11* deletion leads to stabilization of HIF1a under normoxic conditions and increases its downstream target gene expression. To investigate how HIF1a is stabilized in $MPL^{W515L}/Stk11^{\Delta/\Delta}$ cells, we assayed for levels of prolyl hydroxylase 2 (PHD2) and hydroxylated HIF1a. In the mutant cells, hydroxylation of HIF1a was reduced compared to controls while PHD2 was largely unchanged, suggesting an impairment of PHD activity in these cells (Fig 9B).

Next, to determine whether stabilization of HIF1a is sufficient to promote enhanced self-renewal, we transduced wild-type murine bone marrow cells with combinations of MPL^{W515L}, wild-type HIF1a and an allele of HIF1a (HIF1aPP/AA) that cannot be hydroxylated and targeted for VHL-mediated ubiquitination [123]. Consistent with a key role for HIF1a in the replating phenotype of cells with activated JAK/STAT signaling, we found that HIF1a stabilization was sufficient to confer serial replating of MPL^{W515L} cells with wild-type STK11 expression (Fig 9C). Together, these data confirm that HIF1a stabilization is sufficient for enhanced self-renewal of cells expressing MPL^{W515L}. Prior studies have indicated that mitochondrial function through OXPHOS and production of mitochondrial reactive oxygen species (mitoROS) has been linked to the stabilization of HIF1a [124-126]. Consistent with our prediction that HIF1a is stabilized through increased mitoROS, we also observed that the levels of mitoROS were elevated in $Jak2^{V617F}/Stk11^{\Delta/\Delta}$ cells (Fig 9D).

Finally, we assayed whether the replating of $MPL^{W515L}/Stk11^{\Delta/\Delta}$ cells was sensitive to drugs known to target HIF1a through various mechanisms: disruption of HIF1a DNA binding (echinomycin), inhibition of mTOR (rapamycin), and reduction of mitochondrial ROS (Mitotempo and S3QEL 2). We observed that colony formation was inhibited by all four compounds, with the most significant decrease caused by Mitotempo (Fig 9E). Furthermore, targeting mitochondrial superoxide with Mitotempo resulted in both strong inhibition of colony formation and HIF1a destabilization while suppression of complex III-derived superoxide without alteration of OXPHOS with S3QEL-2[127] was still sufficient to inhibit

colony formation and HIF1a protein stabilization (Fig 9E). By contrast, sequestration of cellular ROS by N-acetylcysteine failed to impede replating (Fig 9F). Taken together our data are consistent with the model that loss of LKB1 leads to increased mitochondrial ROS signaling which increases stabilization of HIF1a and enhances self-renewal.

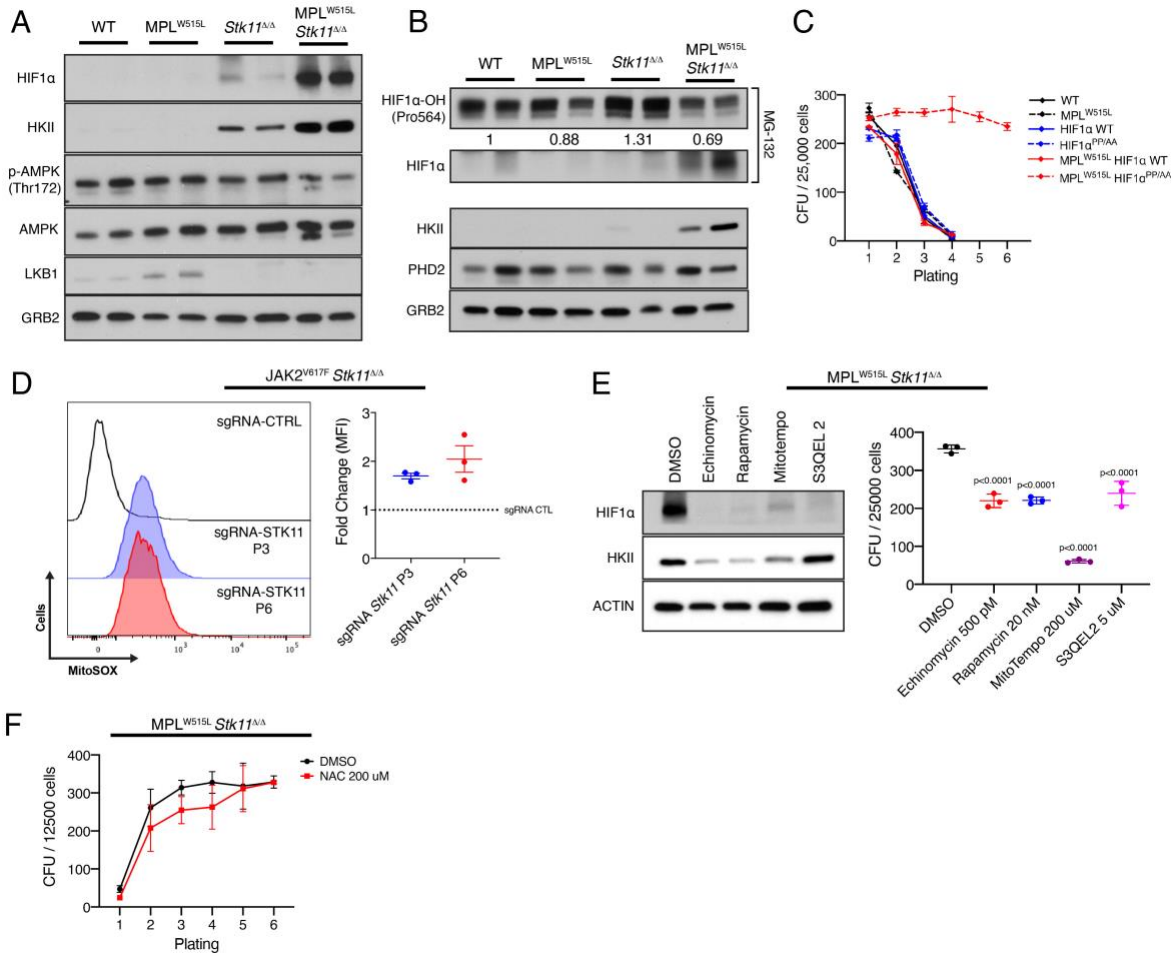

Figure 10: Stabilization of HIF1a promotes colony formation in cells with MPL^{W515L} that are deficient for *Stk11*. A) Western blot analysis of protein levels in hematopoietic cells after the first plating. GRB2 is shown as the loading control. n=2 B) Western blot analysis of HIF1a hydroxylation and PHD2 after the first plating. Densitometry is showed relative to WT. GRB2 is displayed as the loading control. n=2 C) Colony forming units over

6 generations in wild type cells transduced with MPL^{W515L}, HIF1a WT, HIF1a PP/AA mutant and the various combinations. The average plus/minus SEM are shown, n=2 D) Comparison of mitochondrial ROS in cells at platings 1, 3 and 6. The average plus/minus SEM are shown. E) (Left) Western blot analysis of protein levels in MPL^{W515L}/*Stk11*-null cells after treatment with various small molecules known to target HIF1a stabilization. Actin is shown as a loading control. (Right) Effect of small molecules on colony formation capacity of MPL^{W515L}/*Stk11*-null cells. The average plus/minus SD are shown. P values by Dunnet's multiple comparisons test against DMSO control. F) Effect of N-acetylcysteine (NAC) on the colony re-plating phenotype. No significant differences were observed. The average plus/minus SEM are shown, n=3

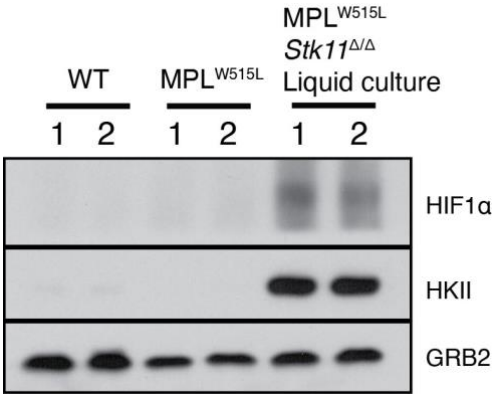

Supplemental Figure 4: Western blot of HIF1a and hexokinase II (HKII) in MPL^{W515L}/*Stk11*-null cells in liquid culture. GRB2 is displayed as loading control. Two biological replicates are shown next to one another for each genotype.

3.4 Loss of Stk11 transforms MPLW515L induced MPN to spent phase with immature blasts in vivo

Serial replating is often used as an in vitro surrogate for leukemic transformation, but there are examples which show that these are not always inexorably linked. To study whether the potent re-plating phenotype seen with deletion of *Stk11* is associated with in vivo transformation, we modeled heterozygous and homozygous loss in animal models of MPNs. First, we bred *Jak2*^{V617F} inducible mice with Vav-Cre and the *Stk11*-floxed strains. As expected, *Jak2*^{V617F}/Vav-Cre animals developed an MPN characterized by polycythemia and succumbed to disease by 220 days, with 50% lethality seen at day 150 days (Fig. 10A,B). Loss of *Stk11* did not appreciably alter the peripheral blood counts, but significantly impaired survival, with all mice succumbing to disease by 120 days with 50% lethality seen at day 75. Of note, heterozygous loss of *Stk11* had no phenotype, consistent with prior reports [117-119]. Furthermore, activation of JAK/STAT signaling in vivo led to an increase in the $Lin^{-}Sca^{+}c\text{-}Kit^{+}$ HSC fraction and a modest decrease in $Lin^{-}Sca^{+}$ progenitors, with no change in the proportion of myeloid progenitors, simultaneous deletion of one allele of *Stk11* did not alter these phenotypes (Fig 10C-E).

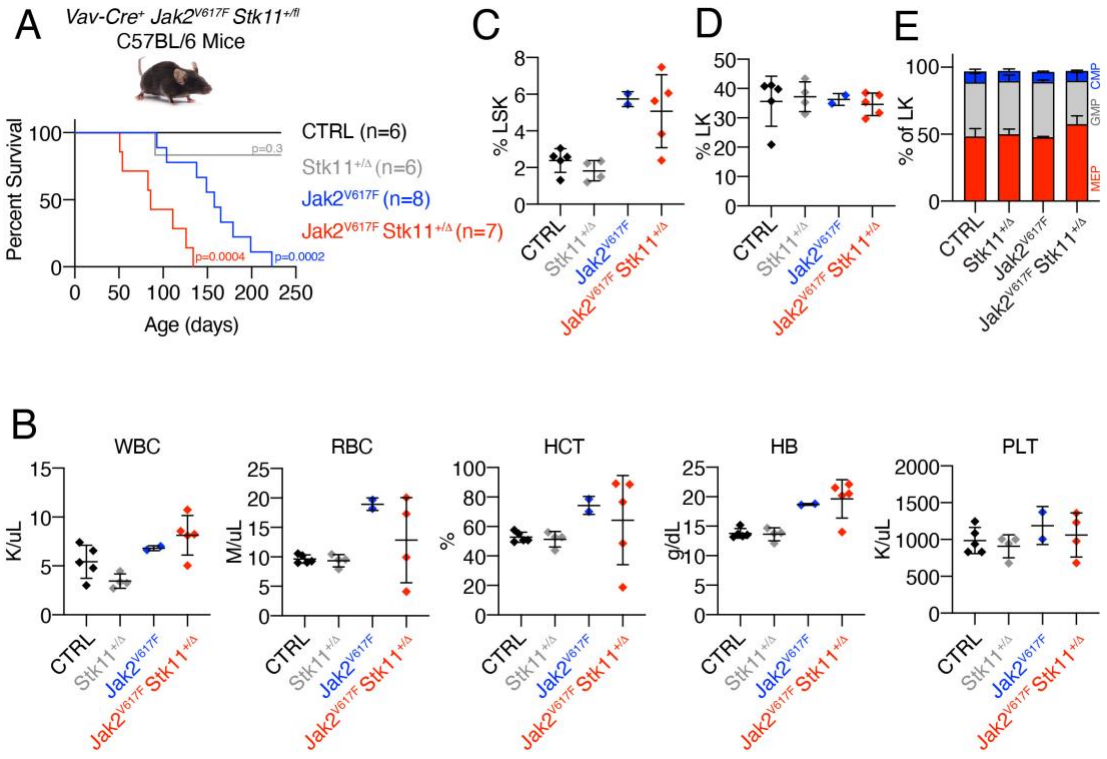

Figure 11: Heterozygous deletion of *Stk11* enhances the MPN phenotype in *Jak2*^{V617F}/Vav-Cre mice. A) Survival curve for four different groups of animals: *Jak2*^{V617F}/*Stk11*$^{+/\Delta}$/Vav-Cre; *Jak2*^{V617F}/Vav-Cre; *Stk11*$^{+/\Delta}$/Vav-Cre; and *Stk11*$^{fl/+}$ or *Jak2*^{V617F} without Cre control (CTRL) animals. p=0.0013 for the survival difference between *Jak2*^{V617F}/Vav-Cre and *Jak2*^{V617F}/*Stk11*$^{fl/+}$/Vav-Cre mice. The p values in the figure refer to the differences between the control and the experimental groups. B) Peripheral blood counts for the four different genotypes at 2 months of age. C-E) Percentages of LSK (C), LK (D) and myeloid progenitor cells (E) in mice of the four different genotypes. Taken at 2 months. The average +/- SD are shown.

Next, to assess the effect of complete LKB1 loss after MPN development, we collected HSPCs from Mx1-Cre/*Stk11*$^{fl/fl}$ or *Stk11*$^{fl/fl}$ control animals without Cre, transduced with

MPL^{W515L}-eGFP and transplanted the cells to irradiated congenic animals (Fig 11A). After three weeks, when the animals displayed features of an MPN, we confirmed that the presence of two floxed *Stk11* alleles did not alter the engraftment efficiency (Fig S5A). We then treated the mice with three doses of pIpC to induce *Stk11* deletion and observed that loss of *Stk11* led to rapid lethality, reduced body and spleen weights and pancytopenia (Fig 11B-D). Histological analysis of the MPL^{W515L}/*Stk11*$^{\Delta/\Delta}$ mice at the time of sacrifice revealed that loss of *Stk11* was associated with much more intense fibrosis and osteosclerosis of the bone marrow compared to those mice which retained *Stk11* (Fig 11E,F). Furthermore, in contrast to the MPL^{W515L} group, in which 6 of 7 mice developed MPN, the majority of the MPL^{W515L}/*Stk11* mice (8 of 13) developed a malignancy characterized by a variably hypoceullular bone marrow containing multiple foci of blasts comprising >20% of the mononuclear cells (Fig 11G,H). This disease was also accompanied by minimal to no residual normal bone marrow hematopoiesis and splenic infiltration. By contrast to the heterozygous deletion, complete absence of *Stk11* altered the hematopoietic stem and progenitor cell populations, with a prominent decrease of LK and LSK compartments (Fig 11I). This change was accompanied by an overall decrease in GFP^{+} hematopoietic cells in the bone marrow of MPL^{W515L}/*Stk11*$^{\Delta/\Delta}$ mice (Fig S5B). Finally, we saw increased mitochondrial ROS in the whole bone marrow of MPL^{W515L}/*Stk11*$^{\Delta/\Delta}$ mice (Fig 11J). Although these data are somewhat reminiscent of the *Stk11* knockout bone marrow aplasia phenotype, in the context of mutant JAK2 or MPL, loss of *Stk11* recapitulates critical features of MPN disease progression to acute myeloid leukemia in patients.

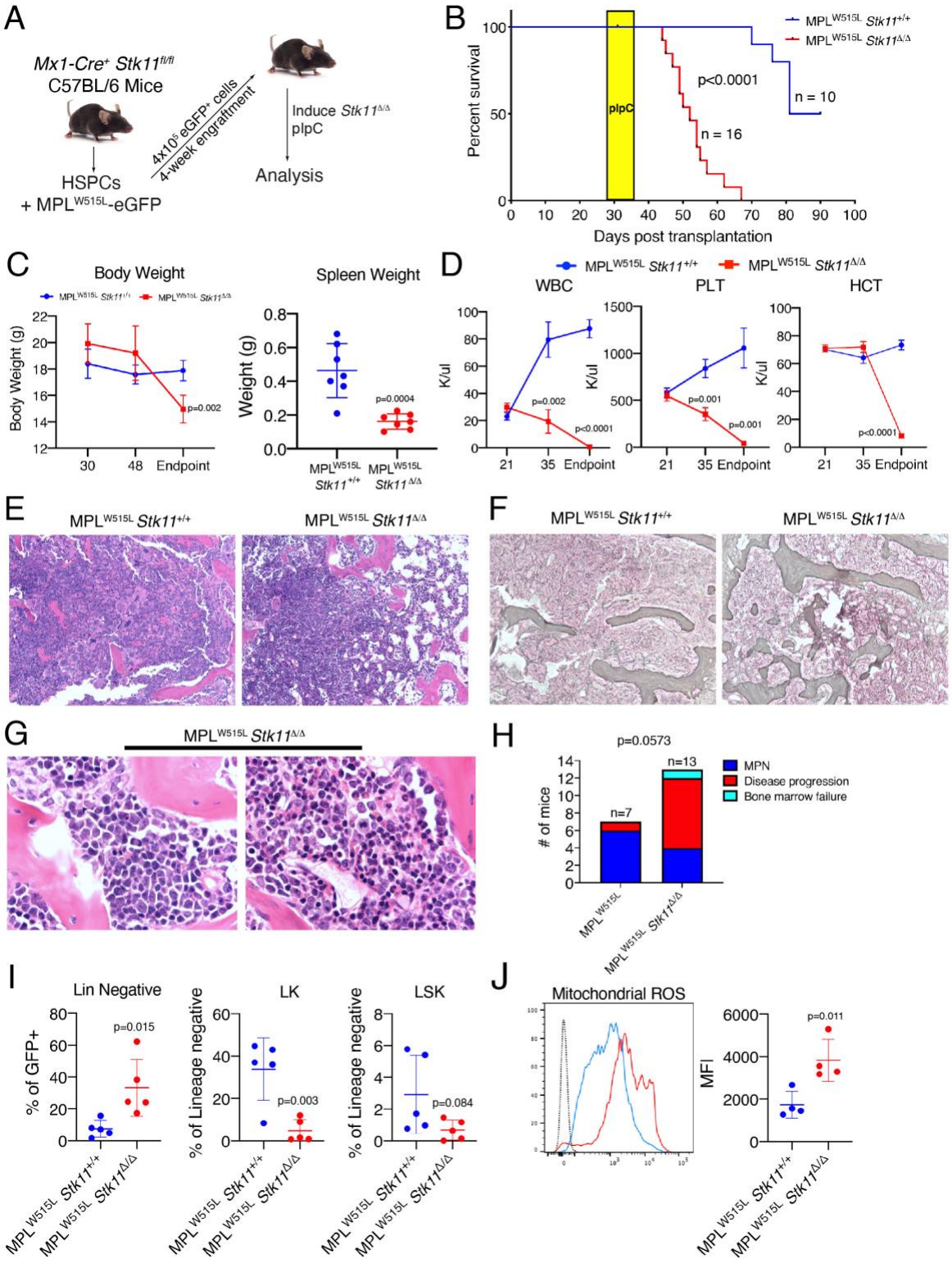
A
Mx1-Cre+ Stk11fl/fl
C57BL/6 Mice
HSPCs
+ MPLW515L-eGFP
4x10^5 eGFP+ cells
4-week engraftment
Induce Stk11Δ/Δ
pIpC
Analysis
B
Percent survival
Days post transplantation
MPLW515L Stk11+/+
MPLW515L Stk11Δ/Δ
pIpC
p<0.0001
n = 10
n = 16
C
Body Weight
Body Weight (g)
p=0.002
Endpoint
Spleen Weight
Weight (g)
p=0.0004
D
WBC
PLT
HCT
K/ul
p=0.002
p<0.0001
p=0.001
p=0.001
p<0.0001
21
35
Endpoint
E
MPLW515L Stk11+/+
MPLW515L Stk11Δ/Δ
F
MPLW515L Stk11+/+
MPLW515L Stk11Δ/Δ
G
MPLW515L Stk11Δ/Δ
H
p=0.0573
# of mice
n=7
n=13
MPN
Disease progression
Bone marrow failure
MPLW515L
MPLW515L Stk11Δ/Δ
I
Lin Negative
% of GFP+
p=0.015
LK
% of Lineage negative
p=0.003
LSK
% of Lineage negative
p=0.084
MPLW515L Stk11+/+
MPLW515L Stk11Δ/Δ
J
Mitochondrial ROS
MFI
p=0.011
MPLW515L Stk11+/+
MPLW515L Stk11Δ/Δ

Figure 12: Deletion of *Stk11* drives progression of MPN in vivo. A) Schematic of experimental workflow. B) Survival curve of animals transplanted with *Stk11*$^{fl/fl}$/MX1-Cre/MPL^{W515L} or *Stk11*$^{fl/fl}$/MPL^{W515L} bone marrow cells. Yellow box indicates timing of pIpC treatment. P value (log-rank test) represents the difference in survival between the two groups of mice. C) Body and spleen weights of the two groups of mice. The average plus/minus SD is shown, n=7. D) White blood cell, platelet counts and hematocrit of mice in the two groups. P values were derived by Student's t-test. The average plus/minus SEM is shown, n=5. E,F) Representative H&E and reticulin stained sections of the bone marrow recipient animals. Original magnification 100X (C,D). G) Higher power magnification of the bone marrow of two MPL^{W515L}/*Stk11*$^{-/-}$ mice highlighting the accumulation of immature blasts. Original magnification 500X. H) Comparison of the malignant phenotypes of MPL^{W515L} versus MPL^{W515L}/*Stk11*$^{-/-}$ mice. MPN, animals with a hypercellular bone marrow with mature cells; Disease progression, animals with >20% blasts in in an otherwise hypocellular bone marrow; Bone marrow failure, animals with a hypocellular marrow and no blasts. Differences in the proportions of the phenotypes in the two groups were evaluated by Fisher's exact test. I) Flow cytometry data for hematopoietic progenitor cells. The average plus/minus SD is shown. P values by student's t-test J) Measurement of mitochondrial ROS in whole bone marrow cells from the mice as determined by intracellular flow cytometry. Representative plot (left) and individual data (right) are shown. The average plus/minus SEM is shown. P value determined by Student's t-test.

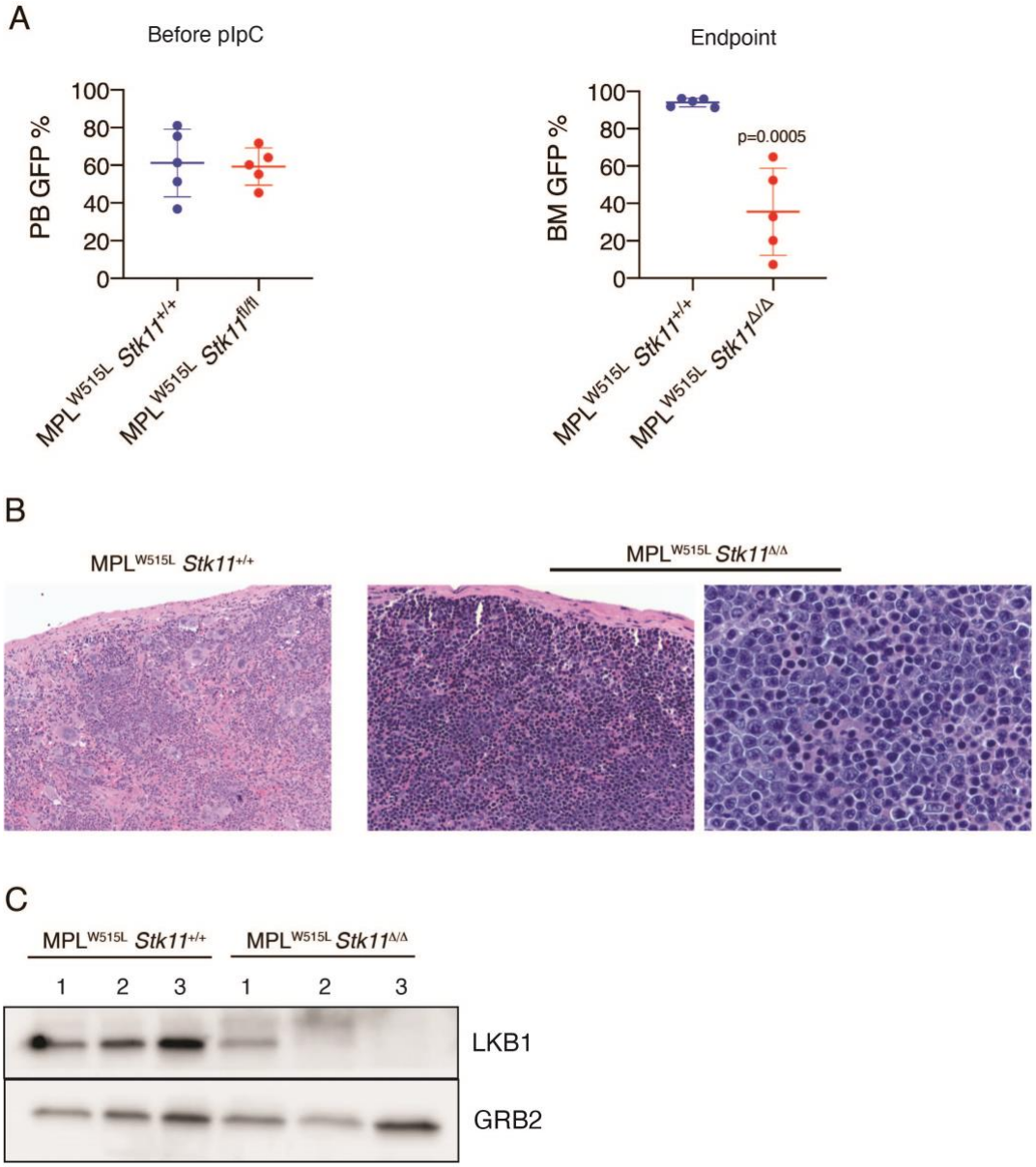

Supplemental Figure 5: Effect of *Stk11* deletion on engraftment of MPL^{W515L} expressing cells in vivo. A) Engraftment of MPL^{W515L}/*Stk11*$^{+/+}$ and MPL^{W515L}/*Stk11*$^{fl/fl}$ donor cells before pIpC treatment at 3 weeks post transplantation as assessed by percentage of GFP^{+} peripheral blood cells. The average +/- SD are shown. B) Engraftment of MPL^{W515L}/*Stk11*$^{+/+}$ and MPL^{W515L}/*Stk11*$^{-/-}$ donor cells at endpoint as assessed by percentage

of GFP^+ bone marrow cells. The average plus/minus SD are shown. C) Western blot of LKB1 in whole bone marrow cells from MPL^{W515L}/*Stk11*$^{+/+}$ and MPL^{W515L}/*Stk11*$^{\Delta/\Delta}$ mice. GRB2 is displayed as a loading control. Protein lysates from three different animals for each group are shown.

3.5 Deletion of STK11 enhances engraftment of human MPN primary cells

We next assayed the consequences of *STK11* depletion of the growth of primary human MPN cells in vivo. We collected peripheral blood $CD34^+$ from patients diagnosed with an MPN, introduced sgRNA targeting *STK11* by nucleofection of RNP particles with Cas9 and then transplanted these cells to NSGS animals (Fig 12A). After 12 weeks, we analyzed engraftment and evaluated the degree of editing of the human cells. Remarkably, we observed a consistent increase in engraftment of cells that showed successful *STK11* gene editing (Fig 12B,C). This was reflected by an increase of human cells in peripheral blood for 2 out of 3 patient samples and an increase of human $CD45^+$ cells in the bone marrow and an increase of total bone marrow cells (Fig 12D). These data indicate that loss of *STK11* increases engraftment of human MPN cells in a xenotransplantation model.

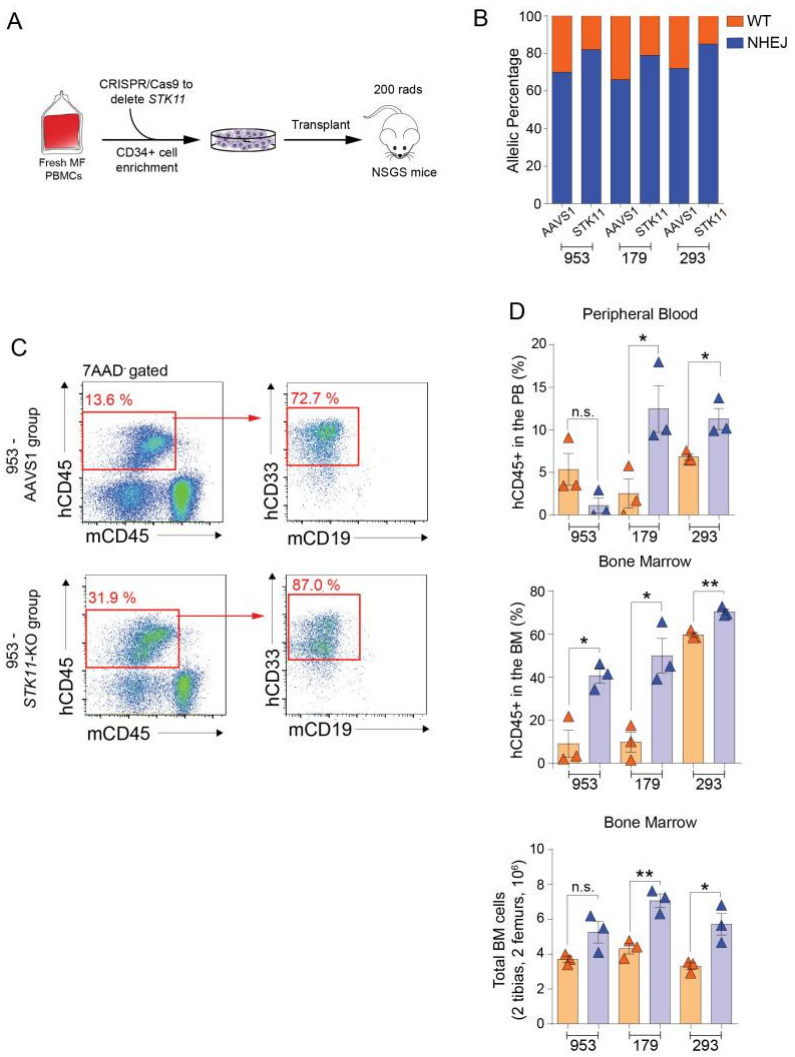

Figure 13: Deletion of *STK11* in human MPN samples increases engraftment in vivo. A) Schematic of the experimental workflow. B) Percentage of non-homologous end joining (NHEJ) after CRISPR editing in three different patient samples**.** C) Flow cytometry plots showing myeloid engraftments in the AAVS1 control versus *STK11*-deleted groups. D) Percentage of human $CD45^{+}$ cells in peripheral blood and bone marrow and total number of bone marrow cells in mice transplanted with cells from 3 different patients. The average +/- SD are shown.

3.6 Loss of STK11 is associated with leukemia progression in human MPNs

We performed a number of studies to determine whether the murine phenotypes observed with *Stk11* loss in cells with activated JAK/STAT signaling are relevant to patients. First, we assayed the mRNA expression level of *STK11* in matched bone marrow specimens from patients at chronic and blast phase MPN. We observed downregulation of *STK11* in all cases, with several patients showing more than a 50% decrease in expression at the blast phase (Fig 13).

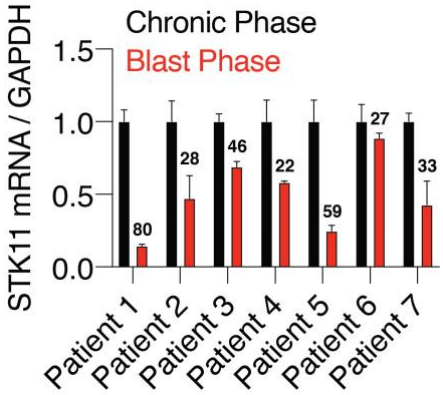

Figure 14: qRT-PCR data comparing the level of *STK11* mRNA in peripheral blood MNCs between matched chronic and blast phase MPN from 7 patients. Numbers indicate the peripheral blood blast percentage in each patient at the blast phase. The average +/- SD are shown. n=3 technical replicates for each patient sample.

Second, to determine whether the level of LKB1 was altered with progression we performed immunohistochemistry on matched bone marrow samples form patients in chronic and blast phase. We observed a consistent and significant decrease in LKB1 staining in the bone marrow (Fig 14A). Together these results confirm that downregulation of LKB1 is a feature of MPN progression. We further stained the same chronic and blast phase sections for HIF1a

and observed increased staining in the blast phase of the disease consistent with LKB1 loss leading to the stabilization of HIF1a (Fig 14B).

Next, to better understand the molecular signatures associated with progression to the blast phase, we performed RNA-seq on matched peripheral blood mononuclear cells from 11 patients who progressed from chronic to blast phase MPN over a period of time ranging from 14 months to 12.4 years. We observed variable separation between the groups by principal component analysis (PCA) and unsupervised clustering, but also some significant variability in both groups. The variation may be due to differences in the genetic composition at the blast stage among the patients, differential timing of disease evolution, or other factors. Both PCA and unsupervised clustering indicated a subset of chronic samples and a subset of blast samples that were clearly well-separated from each other and a smaller number of samples from each group that exhibited intermediate, mixed expression patterns with features of both of the two well-separated subsets. We chose to remove those sample pairs for which one or both of the samples fell in the middle of the distribution with intermediate expression patterns where blast and chronic phase appeared to overlap and focused on 5 well separated pairs (Fig 14C) in order to avoid potential confounders which might not be related to the transition between these two disease states. Unsupervised clustering of these 5 pairs revealed major differences in the transcriptome between the chronic and blast phase of MPN (Fig 14D). To compare the mouse transcriptome of cells overexpressing MPL^{W515L} alone or with *Stk11* loss and the human transcriptome of chronic and blast phase MPN, we performed GSEA using differentially expressed genes in the mouse MPL^{W515L} versus

MPL^{W515L}/*Stk11*$^{\Delta/\Delta}$ comparison and in the human chronic phase versus blast phase MPN as genesets. GSEA showed a strong concordance between human and mouse downregulated genes in the two datasets (Fig 14E). Moreover, GSEA analysis of a published geneset of hypoxia induced genes in CD34^{+} cells[128] revealed enrichment of the hypoxia signature in human blast-phase MPN (Fig. 14F). We also compared normalized enrichment scores from the GSEA analysis in both comparisons. Strikingly, we observed extensive concordance between the pathways enriched in the blast phase of the disease and the ones in MPL^{W515L} cells lacking *Stk11*, including pathways related to hypoxia, oxidative phosphorylation and translation (Fig 14G).

Finally, we treated primary MPN-BP samples and healthy CD34^{+} controls with drugs targeting the HIF, mTOR and JAK/STAT pathways. Echinomycin and Mitotempo were tested based on our observation that they led to destabilization of HIF1a in cells with MPL^{W515L} that lack LKB1 (Fig 9E). We also tested PT2977, a small molecule that inhibits HIF2a[129], as well as the mTOR pathway inhibitor PP242 and the JAK2 inhibitor ruxolitinib. With the exception of the highest doses of Mitotempo and ruxolitinib, the drugs had no significant effect on colony formation by healthy CD34^{+} cells (Fig 14H). By contrast, we observed consistent, dose-dependent inhibition of colony formation of the five primary MPN-BP specimens with all compounds, with the most striking effects caused by echinomycin and Mitotempo (Fig 14I). Of note, the cells were largely resistant to ruxolitinib with little discrimination between the MPN-BP and healthy CD34^{+} cells, consistent with the

poor activity of this drug in MPN-BP patients. Together, these results suggest that drugs which target the HIF pathway should be considered in this disease.

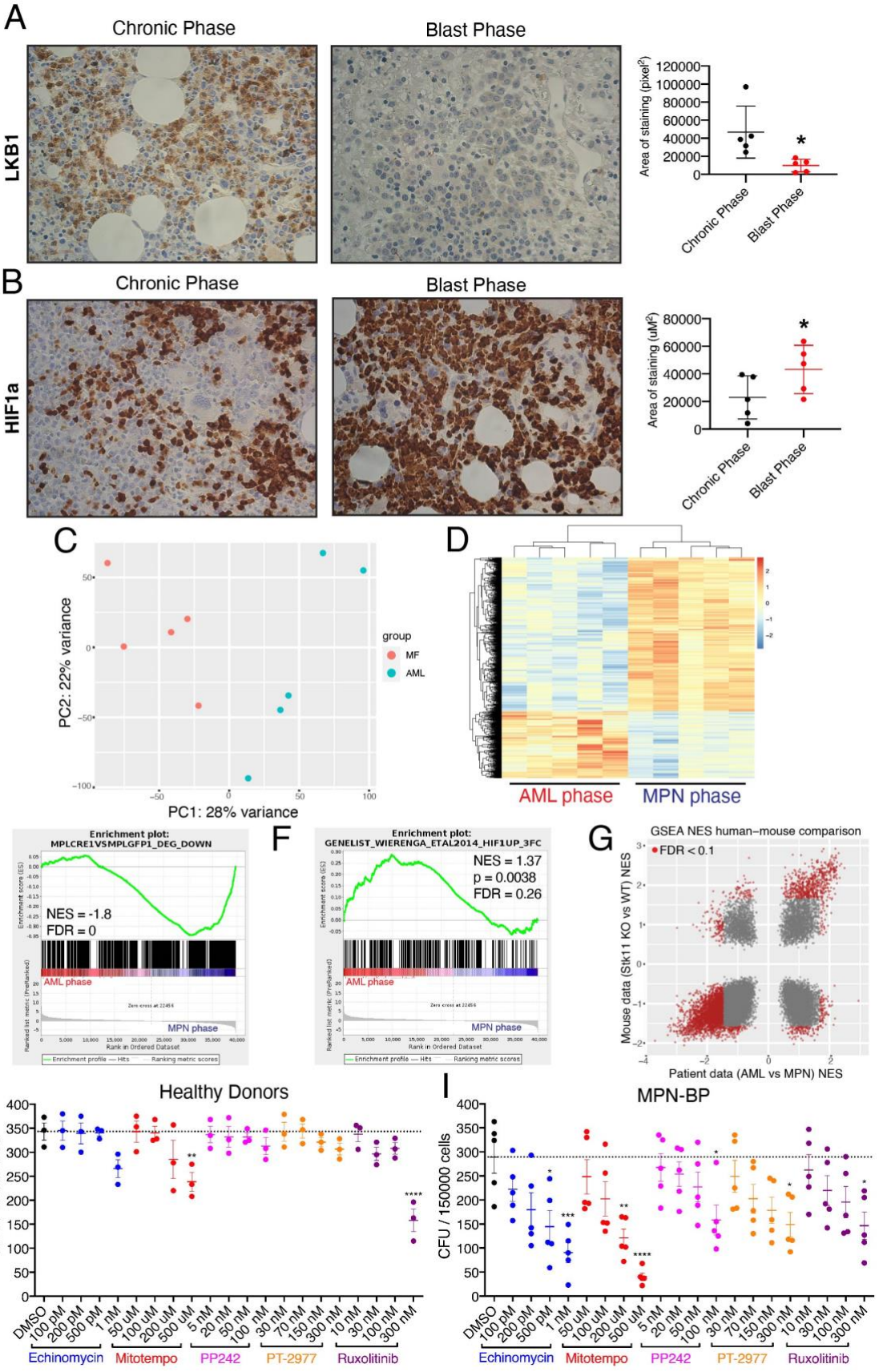
A
Chronic Phase
Blast Phase
LKB1
Area of staining (pixel²)
120000
100000
80000
60000
40000
20000
0
Chronic Phase
Blast Phase
B
Chronic Phase
Blast Phase
HIF1a
Area of staining (uM²)
80000
60000
40000
20000
0
Chronic Phase
Blast Phase
C
PC2: 22% variance
PC1: 28% variance
group
MF
AML
D
AML phase
MPN phase
E
Enrichment plot:
MPLCRE1VSMPLGFP1_DEG_DOWN
NES = -1.8
FDR = 0
AML phase
MPN phase
Rank in Ordered Dataset
F
Enrichment plot:
GENELIST_WIERENGA_ETAL2014_HIF1UP.3FC
NES = 1.37
p = 0.0038
FDR = 0.26
AML phase
MPN phase
Rank in Ordered Dataset
G
GSEA NES human–mouse comparison
FDR < 0.1
Mouse data (Stk11 KO vs WT) NES
Patient data (AML vs MPN) NES
H
Healthy Donors
CFU / 10000 cells
DMSO
100 pM
200 pM
500 pM
1 nM
50 uM
100 uM
200 uM
500 uM
5 nM
20 nM
50 nM
100 nM
30 nM
70 nM
150 nM
300 nM
10 nM
30 nM
100 nM
300 nM
Echinomycin
Mitotempo
PP242
PT-2977
Ruxolitinib
I
MPN-BP
CFU / 150000 cells
DMSO
100 pM
200 pM
500 pM
1 nM
50 uM
100 uM
200 uM
500 uM
5 nM
20 nM
50 nM
100 nM
30 nM
70 nM
150 nM
300 nM
10 nM
30 nM
100 nM
300 nM
Echinomycin
Mitotempo
PP242
PT-2977
Ruxolitinib

Figure 15: LKB1 loss is a feature of human MPN. A) IHC for LKB1 in bone marrow sections from chronic and blast phase MPN. Left, representative IHC; right, Area of staining quantification for 5 paired samples. Original magnification, 400X. The average plus/minus SD are shown. *, p value <0.05). B) IHC for HIF1a in bone marrow sections from chronic and blast phase MPN. Left, representative IHC; right, Area of staining quantification for 5 paired samples. Original magnification, 400X. Images from B and C are from the same patient. C) Principal component analysis of RNA-sequencing data from 5 paired samples of chronic phase MPN and blast phase MPN. D) Unsupervised clustering of differentially expressed genes between chronic phase and blast phase MPN. E) GSEA analysis of downregulated genes in mouse RNA-seq against human RNA-sequencing dataset. F) GSEA analysis revealing enrichment of a published hypoxia related geneset[128]. G) Comparison of normalized enrichment scores (NES) of all pathways between the mouse and human RNA-seq datasets. Significance at FDR < 0.1. H) Number of hematopoietic colonies generated by $CD34^+$ progenitors from healthy donors treated with echinomycin, Mitotempo, PP242, PT2977 and ruxolitinib at various concentrations versus DMSO control. Dotted line represent mean of the DMSO control. **p=0.0044 for Mitotempo at 500 μM, ****p<0.0001 for ruxolitinib at 300 nM. All comparisons by Dunnet's multiple comparisons test versus DMSO control I) Number of hematopoietic colonies generated by peripheral blood mononuclear cells from MPN-BP patient samples treated with Echinomycin, Mitotempo, PP242, PT2977 and ruxolitinib at various concentrations versus DMSO control. Dotted line represent mean of the DMSO control. *p=0.0119 and ***p=0.0001 for Echinomycin at 500 pM and 1 nM, respectively. **p=0.0020 and ****p<0.0001 for Mitotempo at 200 μM and

500 μM, respectively. *p=0.0312 for PP242 at 100 nM. *p=0.0161 for PT2977 at 300 nM. *p=0.0136 for Ruxolitinib at 300 nM. All comparisons by Dunnet's multiple comparisons test against DMSO control. The average plus/minus SEM are shown.

3.7 Discussion

Loss of *Stk11* is a key event in the progression of several solid malignancies as well as the dominant genetic mutation that leads to Peutz-Jeghers syndrome, characterized by increased risk of cancer development[130]. Prior studies have shown that loss of LKB1 in hematopoietic cells leads to an initial burst of proliferation of HSPCs followed by bone marrow failure as opposed to tumor development[117-119]. Our findings that LKB1 loss imparts enhanced self-renewal of cells with activated JAK/STAT signaling strongly suggest that continued stimulation of this pathway allows for growth of HSPCs that lack LKB1.

Deletion of *Stk11* in MPN cells induced expression of genes related to hypoxia and mitochondrial function. At the molecular level, stabilization of HIF1a under normal oxygen tension was a striking feature of *Stk11* deleted MPN cells: this effect is shared with a mouse model of Peutz-Jeghers syndrome and mouse embryonic fibroblasts[131,132]. HIF1a is a transcriptional factor widely known for its role in solid malignancies where it is consistently stabilized to promote tumor cell survival under hypoxia, tumor angiogenesis and cell proliferation. In hematopoietic cells with enhanced JAK/STAT signaling, HIF1a promotes self-renewal of MPN cells likely through induction of genes related to stemness and proliferation. With respect to the link between LKB1 loss and HIF1 stabilization, increased

mitochondrial ROS produced by the electron transport chain during OXPHOS has been linked to the stabilization of HIF1a in hypoxia[124,125]. We surmise that the observed increase in mitochondrial ROS impairs the normal prolyl hydroxylase function needed for VHL-mediated HIF1a ubiquitination and degradation by the proteasome.

A number of genetic alterations have been modeled in mouse models of MPN to mimic the alterations found in the human blast phase MPN including loss of *TP53* and *JARID2*. We show that deletion of *Stk11* in the MPL^{W515L} mouse model of MPN resulted in increased lethality due to a spent phase MPN phenotype with intense osteosclerosis and bone marrow fibrosis, accompanied by pockets of immature blasts. Of note, deletion of *STK11* in primary myelofibrosis (PMF) patient samples and transplantation in NSGS recipients caused an increase in human myeloid cell engraftment, rarely seen in PMF xenografts, but no overt leukemia suggesting that additional mutations present in the patient samples may cooperate with *STK11* loss to produce a leukemic phenotype in humans.

Of note, the two libraries contained sgRNAs that target a number of genes associated with MPN progression and myeloid leukemia, including *TET2*, *ASXL1*, *EZH2*, and *DNMT3A*. It is notable that none of these sgRNAs were enriched in *JAK2* mutant cells at platings 3 or 5. Although this may be a consequence of poor gene editing, it suggests that loss of these genes individually does not confer enhanced self-renewal and argues that *STK11* is a more potent tumor suppressor in the MPNs.

Pseudo-hypoxia and stabilization of HIF1a have been recently described in MDS and MPN chronic phase[133,134]. With respect to the latter observation, there was only a modest increase in HIF1a levels and this was observed primarily in MPN cell lines which have been derived from patients with blast phase disease. Our IHC data reveal that HIF1a is present at the chronic phase, but that it is greatly increased at the blast phase, and our RNA-seq data demonstrate that HIF-induced pathways are markedly enriched in the leukemia phase.

Our findings provide insights into potential therapeutic approaches to better treat blast phase disease. Mice that lack HIF1a did not develop any detrimental phenotype under steady state conditions, suggesting that is a viable target[135]. Moreover, recent developments in structure-based design approaches for drug discovery made possible the identification of a selective HIF2a antagonist, PT2399, which can dissociate HIF2a from his partner HIF1b, preventing its translocation to the nucleus[136]. It has been reported that PT2399 provides on target efficacy in both in vitro and in vivo pre-clinical studies of kidney cancer[136]. Here we demonstrate that PT2977, a potent and selective analog of PT2399 that is being investigated in an open-label Phase 2 study of Clear Cell Renal Carcinoma, selectively inhibited colony formation of MPN-BP cells, which demonstrate stabilization of both HIF1a and HIF2a. Thus, our work lends strong rationale for the use of HIF inhibitors in the leukemia phase of the MPNs.

CHAPTER IV

CONCLUSIONS AND FUTURE DIRECTIONS

Ruxolitinib and the more recent Fedratinib remain the primary targeted therapies for the treatment of PMF. Despite having clinical efficacy by improving symptoms and reducing splenomegaly, Ruxolitinib does not reduce significantly the allele burden, does not reduce bone marrow fibrosis and it is frequently discontinued due to acquired resistance. Therefore a major challenge remains to find alternative ways to target the malignant clone.

The importance of the megakaryocyte lineage in the maintenance of normal hematopoietic stem cell quiescence suggests that dysplastic megakaryocytes in PMF may fuel expansion of malignant clones that sustain the disease and promote bone marrow fibrosis through inflammatory cytokines.

The phase I clinical trial presented in this thesis suggests that targeting megakaryocytes through inhibition of AURKA with Alisertib is able to increase megakaryocyte differentiation through polyploidization and reduce bone marrow fibrosis. It remains to be determined if the improvement of megakaryocyte morphology and increased expression of GATA1 in the bone marrow is due to recovery of normal hematopoietic clones or improved differentiation of mutant PMF clones. Laser-capture microdissection of GATA1 positive megakaryocytes in bone marrow sections and DNA sequencing will help determine how Alisertib treatment impacts megakaryocyte differentiation in human specimens. Furthermore, it will be important to assess the efficacy of a combination therapy using Ruxolitinib and Alisertib and assess their effects on allele burden in PMF patients.

Progression to blast-phase MPNs remain a serious complication with dismal prognosis for MPN patients. Identification of mechanisms of transformation is a key aspect in determining

ways to target the leukemic clone or preventing transformation. The CRISPR/Cas9 approach used in this thesis revealed a role for STK11/LKB1 in the leukemic transformation of MPNs through upregulation of hypoxia inducible proteins. Interestingly, loss of STK11/LKB1 alone results in HSC exhaustion while cooperation with the JAK-STAT oncogenic driver increases self-renewal of MPN cells. It will be important to investigate how hyperactivation of the JAK-STAT pathway leads to cell survival. Overexpression of wild type or catalytically inactive STK11/LKB1 in STK11/LKB1 null HSPCs with or without JAK-STAT activation coupled with proteomic approaches will help define critical STK11/LKB1 interactors that mediate the self-renewal phenotype. In addition, given the strong effect of STK11/LKB1 on mitochondrial function, it will be important to isolate mitochondria from hematopoietic cells and characterize changes in the mitochondrial proteome. Moreover, it will be important to determine the efficacy of hypoxia inducible proteins inhibition through reduction of mitochondrial ROS by Mitotempo *in-vivo* or through inhibition of HIF2a with PT2977. This can be achieved in the *MPL*^{W515L} *Stk11* null model as well as in MPN-BP patient derived xenografts models.

Finally, it will be important to understand the mechanism by which STK11/LKB1 is downregulated in human MPN-BP. Since no recurrent mutations or increase in methylation have been reported for the *STK11* gene in AML, it is possible that epigenetic alterations contribute to the decreased *STK11* expression. Analysis of potential cooperating mutations in epigenetic regulators will help define chromatin accessibility and histone marks changes in the *STK11* gene locus.

CHAPTER V

MATERIALS AND METHODS

5.1 Materials and methods related to chapter II

Patients

Included patients had a confirmed diagnosis of PMF, post-ET/MF or post-PV/MF, were intermediate I risk or beyond by the Dynamic International Prognostic Scoring System (DIPSS) and were in need of treatment; intolerant or refractory to ruxolitinib (or other investigational JAK inhibitors) or unlikely to benefit from ruxolitinib. The study was approved by the institutional review boards at Northwestern University, the Mayo Clinic and the University of Miami, and all patients signed informed consent.

Blood samples processing, $CD34^+$ cell culture and megakaryocyte differentiation

20 mL of peripheral blood (PB) were collected from patients before starting treatment and at the end of each treatment cycle and processed within 24 hours post-collection. For cytokine profiling, 1 mL of PB was used to collect the serum fraction by 2-step centrifugation. PB was centrifuged at 1000 g for 20 minutes sediment the cellular component and the supernatant collected and spun at 2000 g for 10 minutes to obtain the serum fraction. Serum fractions were stored frozen at -80 C until use.

The remaining PB was used for isolation of CD34+ hematopoietic progenitors, which are known to be increased in PB of PMF patients. Initially, PB was diluted 1:1 with PBS in a 50 mL conical tube and then 15 mL of Ficoll (GE healthcare) was laid on the bottom of the tube for density gradient centrifugation at 400 g for 30 minutes at room temperature (RT). After

centrifugation erythrocytes are found at the bottom of the tube while the mononuclear cell fraction is contained within the buffy coat. The mononuclear cell fraction (MCF) is collected and washed with PBS. After centrifugation the MCF is subjected to CD34+ positive selection using the Miltenyi Biotech MACS system. The MCF is resuspended with 300 ul of PBS supplemented with 0.5% BSA and 2 mM EDTA, 100 ul of FCR blocker and 100 ul of CD34+ microbeads and incubated at 4 C for 30 minutes. After incubation, cells are passed through an LS column (Miltenyi Biotech) on a magnetic stand. Columns are washed 3 times with PBS supplemented with 0.5% BSA and 2 mM EDTA and the negative fraction collected and frozen. The CD34+ positive fraction was flushed out of the column with a plunger.

CD34+ cells were cultured initially under conditions to favor expansion using StemSpan Media (Stemcell technologies) supplemented with 50 ng/mL human IL-6, 100 ng/mL human FLT-3, 50 ng/mL human SCF and 30 ug/mL human low-density lipoprotein (LDL). After 5 days of expansion, megakaryocyte differentiation was performed by culturing CD34+ cells in 1:1 RPMI1640 media (Gibco, Thermo Scientific) and StemSpan Media supplemented with 50 ng/mL mouse thrombopoietin (TPO). Cells were expanded every 2 days by dilution in other wells of the plate to avoid overcrowding of the culture.

In vitro treatment of megakaryocyte differentiating cultures with ruxolitinib or alisertib

For in-vitro drug treatments, $CD34^{+}$ cells at the end of the 5 day expansion phase were cultured in 10% FBS in RPMI1640 media supplemented with 50 ng/mL mouse

thrombopoietin in the presence of various concentrations of either ruxolitinib or alisertib for 72 hours. After 72 hours megakaryocyte differentiation was assessed by Hoechst 33342 (Invitrogen) staining at a concentration of 5 ug/mL for 1 hour at 37°C with 5% CO_2 for DNA content analysis. Apoptosis was assessed by Annexin V staining. Cells were initially stained with antibodies against human CD41 and human CD42. After the staining, cells were washed with staining buffer (PBS supplemented with 0.5% BSA and 2 mM EDTA), resuspended in Annexin V staining buffer (BD biosciences) with Annexin V-FITC at a 1:10 dilution and incubated for 15 minutes at RT. Flow cytometric analysis was performed on an LSRII flow cytometer (BD) and post-acquisition analysis performed with FlowJo. Cells were gated for Forward Scatter (FSC) and Side Scatter (SSC), doublets excluded by Forward Scatter Area (FSC-A) and Forward Scatter height (FSC-H). Mature megakaryocytes were identified by gating on CD41+ CD42+ cells and differentiation by ploidy was evaluated by selecting Hoechst 33342 peaks greater than 4N. Apoptosis was assessed as percentage of Annexin V positive cells in the CD41+ CD42+ megakaryocyte gate.

Luminex cytokine array and TGF-β ELISA

To assess multiple cytokines in a single sample, a ProcartaPlex immunoassay (Invitrogen, Thermo Scientific) was used to assess 45 different cytokines in the serum of patients pre- and post-therapy. PB-derived serum samples were thawed on ice and centrifuged at 10000 g for 5 minutes. Magnetic beads for the multiplex assay were prepared according to the manufacturer instructions and added to a 96 well plate. Samples and blanks were added to the beads and incubated overnight at 4ºC. After two plate washes, detection antibody was

added to the samples and incubated for 30 minutes at RT. The plate was washed again two times, incubated with Streptavidin-PE for 30 minutes at RT and washed two times. Beads were resuspended in 120 ul of Reading Buffer and reading performed on a Luminex 200. To assess active TGF-β1 levels 1N HCl was added to the serum to activate latent TGF-β1 form and then the acidified sample was neutralized with 1.2 N NaOH/0.5 M HEPES. The sample was diluted 20-fold and assayed with a Quantikine ELISA kit (R&D Systems) according to the manufacturer instructions. The plate was read using a microplate reader set at 450 nm. A standard curve was generated by four parameter logistic (4-PL) curve fit and unknown values interpolated from the standard curve.

GATA1 Immunohistochemistry

GATA1 staining of sections of bone marrow biopsies was performed using an anti-GATA1 antibody (CST, catalog number 3535) as previously described[34]. The percentage of GATA1 positive megakaryocytes represents the number of positively stained cells relative to the total number of megakaryocytes. A minimum of 100 megakaryocytes were counted, with the exception of 42-10, where limited tissue was available. Images were obtained with an Olympus BX41 microscope fitted with a Jenoptik ProgRes Speed XT camera.

5.2 Materials and methods related to chapter III

Mice

All animals were of the C57BL/6 background. *Jak2*^{V617F} knock-in (Cat# JAX:031658, RRID:IMSR_JAX:031658), *Stk11*floxed (Cat# JAX:014143, RRID:IMSR_JAX:014143), Vav-Cre (Cat# JAX:008610, RRID:IMSR_JAX:008610), Mx1-Cre (Cat# JAX:003556, RRID:IMSR_JAX:003556) and Rosa26-Cas9 knock-in mice (Cat# JAX:026175, RRID:IMSR_JAX:026175) were purchased from Jackson Laboratories. NSGS mice (Cat# JAX:013062, RRID:IMSR_JAX:013062) were purchased from Jackson Laboratories. All mice were genotyped for the presence of the correct alleles by PCR. Animal studies were approved by the Northwestern University IACUC and the Washington University IACUC.

Patient Samples

All specimens were studied with approval by the Institutional Review Boards of Northwestern University, Memorial Sloan Kettering, Washington University, and the Mayo Clinic.

CRISPR/Cas9 screen

We generated a mouse sgRNA library for CRISPR-KO with 4X coverage targeted against the genes listed in the Uniprot Curated List of Tumor Suppressors as well as several MPN associated genes (Table S1). Given that loss of *TP53* has been previously reported to be a transforming event in MPN to AML[47], we did not include this gene in the library. To perform

the screen, lineage-negative HSPCs were isolated from bone marrow of *Jak2*^{V617F}/Vav-Cre/Cas9 or Vav-Cre/Cas9 mice and transduced with either of two lentiviral sgRNA libraries or empty vector control at multiplicity of infection of 0.5. Transduced cells were selected from 24 hours with 2 ug/mL blasticidin (Sigma-Aldrich, 15205) and then plated on M3434 methylcellulose media (Stem Cell Technologies, M3434) with 1 ug/mL blasticidin. Every 7 days of culture, colonies were enumerated and cells recovered for serial replating over 5 generations. DNA of cells from platings 1, 3 and 5 was extracted with GenElute™ Mammalian Genomic DNA Miniprep Kit (Sigma-Aldrich, G1N70) and next generation sequencing was performed to evaluate enrichment of guide RNAs of plating 3 and 5 against plating 1 as a baseline. sgRNA enrichment was determined using PinAPL-Py[137]

sgRNA/Cas9 RNP delivery

Gene editing with Cas9 ribonucleoprotein complexes (RNP) was achieved using the Alt-R CRISPR-Cas9 system (IDT). Briefly, equimolar amounts of crRNAs targeting mouse *Stk11* or/and trcrRNA were annealed to form the gRNA. Non-targeting control crRNA #1 (IDT) was used for control conditions. 18 pmol of recombinant Cas9 (IDT, 1081061) were combined with 22 pmol of gRNA to form RNP complexes, which were then delivered to c-kit^{+} HSPCs using the NEON electroporation system (Thermo Scientific) with settings 1700 V, 20 ms, 1 pulse as described previously[138]. After 24 hours, cells were plated in M3434 methylcellulose media (Stemcell Technologies) and serially replated every 7 days over 6 generations. The serial replating was performed by diluting methylcellulose 1:1 with PBS to

recover the cells. After centrifugation, cells were counted and the same number of cells plated in M3434 methylcellulose media.

Viral Transduction

High titer retrovirus was obtained by transfecting Platinum E cells (Cell Biolabs, RV-101, RRID:CVCL_B488) with 12 ug of retroviral construct using X-tremeGENE 9 transfection reagent (Roche, XTG9-RO) and collecting viral supernatant two times 48 hours and 72 hours post-transfection. Viral transduction was performed by spinoculation; 2-5x 10^6 cells were mixed with virus and 1 μg/ml Polybrene as infection adjuvant and centrifuged for 90 minutes at 2500 RPM at 32 C. Transduction efficiency was evaluated by flow cytometry after 24 hours of culture post-transduction by measuring GFP positive cells.

Flow Cytometry

Bone marrow cells were isolated by crushing long bones with mortar and pestle in phosphate buffered saline (PBS) and filtered through a 70 μm nylon mesh to obtain a single cell suspension. The HSPC compartment was analyzed using and anti-mouse V450-lineage negative antibody cocktail (BD Biosciences Cat# 561301, RRID:AB_10611731), anti-mouse APC-CD117 (BD Biosciences Cat# 553356, RRID:AB_398536), and anti-mouse PE-Cy7-Sca1 (Thermo Fisher Scientific Cat# 25-5981-82, RRID:AB_469669) by incubating bone marrow cells with the antibodies for 30 minutes at 4 C. Flow cytometry was performed on a LSRII flow cytometer (BD Biosciences). To measure mitochondrial ROS, whole bone marrow cells were incubated with 1.5 μm mitoSOX (Thermo Scientific,

M36008) in Earle Balanced Salt Solution (EBSS) supplemented with 0.5% BSA in a tissue culture incubator for 30 minutes, washed with EBSS and immediately analyzed. For colony forming assays with sorted cells, GFP^+ $mCherry^+$ double transduced cells were isolated 36 hours post-transduction by FACS using a FACS Aria II (BD Biosciences).

Transplantation

Bone marrow from *Stk11*$^{fl/fl}$ Mx1-Cre^+ or *Stk11*$^{fl/fl}$ mice was isolated by crushing femurs and tibias and c-kit^+ cells isolated using magnetic enrichment (Miltenyi Biotec CD117 MicroBeads, mouse # 130-091-224) and cultured overnight in Stem Span media supplemented with 50 ng/mL mouse SCF, 10 ng/mL mouse IL-6 and 10 ng/mL mouse IL-3. c-kit^+ cells were then transduced with the MPL^{W515L}-GFP retrovirus by spinoculation and 0.4 x 10^6 GFP^+ cells transplanted into lethally irradiated CD45.1 recipients. MPN development and engraftment was confirmed by CBC and flow cytometry at 3 weeks post-transplantation and pIpC injections performed at 4 weeks post-transplantation for 3 times at increasing dose every other day (2 mg/Kg, 4 mg/Kg, 8 mg/Kg).

Xenotransplantation

Human MF peripheral blood mononuclear cells were isolated with Ficoll (GE Healthcare, Munich, Germany) and mononuclear cells cryopreserved within 24 h after collection in HBSS buffer (Corning #21021CV) containing Pen/Strep (100 Units/mL; Fisher Scientific #MT30002CI), HEPES (10uM; Life Technologies # 15630080) and FBS (2%; Sigma #14009C). For xenotransplantations, $CD34^+$ hematopoietic stem and progenitor cells

isolated were isolated using magnetic enrichment (Miltenyi Biotec # 130-100-453) from $JAK2^{V617F}$ (ID# 953 and 179) or $CALR^{fs}$ (ID# 293) positive MF patients. Enriched $CD34^+$ cells were incubated in SFEMII media (Stemcell technologies #09605) supplemented with Pen-Strep (50 Units/mL), human stem cell factor (SCF; 50 ng/mL), human thrombopoietin (TPO; 50 ng/mL), and human Flt3L (50 ng/mL). 12-24 hr post-sort, $CD34^+$ cells were nucleofected with Cas9/ribonucleorprotein complexed with sgRNA targeting *STK11* as previously described. 48h post nucleofection, these cells were transplanted into sublethally irradiated (200 rads) NOD-scid-Il2rg-null-3/GM/SF (IMSR Cat# JAX:013062, RRID:IMSR_JAX:013062) mice via X-ray guided intra-tibial injections. Engraftment of human cells in xenotransplants were assessed by flow cytometry with antibodies targeting human CD45 (BioLegend Cat# 368511, RRID:AB_2566371) and mouse CD45 (BioLegend Cat# 103139, RRID:AB_2562341) cells.

RNA-sequencing and data analysis

The mRNA-seq on stranded libraries was conducted in the Northwestern University NUSeq Core Facility. Briefly, total RNA examples were checked for quality using RINs generated from Agilent Bioanalyzer 2100. RNA quantity was determined with Qubit fluorometer. The Illumina TruSeq Stranded mRNA Library Preparation Kit was used to prepare sequencing libraries from 100 ng of high-quality RNA samples (RIN>7). The Kit procedure was performed without modifications. This procedure includes mRNA purification and fragmentation, cDNA synthesis, 3’ end adenylation, Illumina adapter ligation, library PCR amplification and validation. lllumina NextSeq 500 sequencer was used to sequence the

libraries with the production of single-end, 75 bp reads at the depth of 20-25 M reads per sample.

Resulting raw sequencing data quality was assessed using FastQC and then the sequencing data was mapped to the mouse UCSC mm10 genome using the STAR RNA-seq aligner (STAR, RRID:SCR_015899). Feature and read summarization was performed using FeatureCounts from the Subread package (Subread, RRID:SCR_009803). Differential expression analysis was performed using EdgeR (edgeR, RRID:SCR_012802) using the QLF test. Gene Set Enrichment Analysis (GSEA, RRID:SCR_003199) was performed on normalized transcript per million (TPM) values from all samples using the GSEA software with the MSigDB gene sets. These RNA-seq data are available in GEO (accession number GSE159737).

RNA-seq analysis of paired patient data

Raw reads were trimmed for quality (threshold of 15) and adapter sequences using version 0.4.5 of TrimGalore (https://www.bioinformatics.babraham.ac.uk/projects/trim_galore), and then aligned to human assembly hg38 with STAR v2.4 using default parameters. Post-alignment quality and transcript coverage were assessed using the Picard tool CollectRNASeqMetrics (http://broadinstitute.github.io/picard/). Raw read count tables were created using HTSeq v0.9.1. Normalization and expression dynamics were evaluated with DESeq2 using the default parameters with library size factor normalization. Potential outliers were removed based on the separation of labeled sample pairs along PC1 of the

principal component analysis. Gene set enrichment analysis (GSEA, RRID:SCR_003199) was run using MSigDB v6 with 'pre-ranked' mode and log2 fold change for pairwise comparisons. Pathway concordance between mouse and human was evaluated by linking gene set names with the normalized enrichment scores and highlighting pathways with FDR < 0.1 in either dataset.

Western blotting

Cells were lysed in RIPA lysis buffer supplemented with halt phosphatase inhibitor cocktail (Thermo Scientific, 78420) and complete protease inhibitor cocktail (Roche). Proteins were separated on a mini protean TGX 4-15% polyacrylamide gel (Bio-Rad) and transferred on a PVDF membrane (Millipore). Antibodies included the following: anti-LKB1 (Cell signaling technologies, Cat# 3050, RRID:AB_823559, Cat# 3047, RRID:AB_2198327), anti-HIF1a (Cell signaling technologies, Cat# 36169, RRID:AB_2799095), anti-HIF2a (Novus, Cat# NB100-122, RRID:AB_10002593), anti-HKII (Cell signaling technologies, Cat# 2867, RRID:AB_2232946), anti-p-AMPKa thr172 (Cell signaling technologies, Cat# 2535, RRID:AB_331250), anti-AMPKa (Cell signaling technologies, Cat# 5832, RRID:AB_10624867), anti-HIF1a-OH Pro564 (Cell signaling technologies, Cat# 3434, RRID:AB_2116958), anti-PHD2 (Novus Biologicals, Cat# NB100-137, RRID:AB_10003054), anti-GRB2 (BD Biosciences Cat# 610112, RRID:AB_397518) and anti-ACTB (Cell signaling technologies, Cat# 3700, RRID:AB_2242334).

Histology

Mouse tissues for histology were fixed in 10% neutral buffered formalin for 24 hours and then processed for H&E staining. IHC was performed using standard protocols with anti-LKB1 (Cell signaling technologies, Cat# 13031, RRID:AB_2716796) and anti-HIF1a (Abcam, Cat# ab16066, RRID:AB_302234) antibodies.

Colony forming unit assays with human MPN-BP cells

150,000 peripheral blood mononuclear cells collected from patients at the blast phase of the disease were plated in H4434 methylcellulose media supplemented with echinomycin (Sigma-Aldrich), Mitotempo (Sigma-Aldrich), PP242 (Selleck Chemicals), PT2977 (MedChem Express) or ruxolitinib at 4 different concentrations. Colonies were enumerated after 14 days. Peripheral blood mobilized $CD34^+$ cells from healthy individuals were similarly cultured with drugs to compare their effects in a non-malignant setting.

References

1 Tomasetti, C., Li, L. & Vogelstein, B. Stem cell divisions, somatic mutations, cancer etiology, and cancer prevention. *Science* **355**, 1330-1334, doi:10.1126/science.aaf9011 (2017).

2 Tomasetti, C. & Vogelstein, B. Cancer etiology. Variation in cancer risk among tissues can be explained by the number of stem cell divisions. *Science* **347**, 78-81, doi:10.1126/science.1260825 (2015).

3 Barbui, T. *et al.* The 2016 WHO classification and diagnostic criteria for myeloproliferative neoplasms: document summary and in-depth discussion. *Blood Cancer J* **8**, 15, doi:10.1038/s41408-018-0054-y (2018).

4 Mehta, J., Wang, H., Iqbal, S. U. & Mesa, R. Epidemiology of myeloproliferative neoplasms in the United States. *Leuk Lymphoma* **55**, 595-600, doi:10.3109/10428194.2013.813500 (2014).

5 Nielsen, C., Birgens, H. S., Nordestgaard, B. G. & Bojesen, S. E. Diagnostic value of JAK2 V617F somatic mutation for myeloproliferative cancer in 49 488 individuals from the general population. *Br J Haematol* **160**, 70-79, doi:10.1111/bjh.12099 (2013).

6 Stein, B. L. *et al.* Age-related differences in disease characteristics and clinical outcomes in polycythemia vera. *Leuk Lymphoma* **54**, 1989-1995, doi:10.3109/10428194.2012.759656 (2013).

7 Stein, B. L. *et al.* Polycythemia Vera: An Appraisal of the Biology and Management 10 Years After the Discovery of JAK2 V617F. *J Clin Oncol* **33**, 3953-3960, doi:10.1200/JCO.2015.61.6474 (2015).

8 Passamonti, F. *et al.* Life expectancy and prognostic factors for survival in patients with polycythemia vera and essential thrombocythemia. *Am J Med* **117**, 755-761, doi:10.1016/j.amjmed.2004.06.032 (2004).

9 Tefferi, A. *et al.* Survival and prognosis among 1545 patients with contemporary polycythemia vera: an international study. *Leukemia* **27**, 1874-1881, doi:10.1038/leu.2013.163 (2013).

10 Tefferi, A. *et al.* Gender and survival in essential thrombocythemia: A two-center study of 1,494 patients. *Am J Hematol* **92**, 1193-1197, doi:10.1002/ajh.24882 (2017).

11 Passamonti, F. *et al.* A prognostic model to predict survival in 867 World Health Organization-defined essential thrombocythemia at diagnosis: a study by the International Working Group on Myelofibrosis Research and Treatment. *Blood* **120**, 1197-1201, doi:10.1182/blood-2012-01-403279 (2012).

12 Lancellotti, S. *et al.* Qualitative and quantitative modifications of von Willebrand factor in patients with essential thrombocythemia and controlled platelet count. *J Thromb Haemost* **13**, 1226-1237, doi:10.1111/jth.12967 (2015).

13 Gunawan, A. *et al.* Ruxolitinib for the Treatment of Essential Thrombocythemia. *Hemasphere* **2**, e56, doi:10.1097/HS9.0000000000000056 (2018).

14 Tefferi, A. Primary myelofibrosis: 2017 update on diagnosis, risk-stratification, and management. *Am J Hematol* **91**, 1262-1271, doi:10.1002/ajh.24592 (2016).

15 Tefferi, A., Litzow, M. R. & Pardanani, A. Long-term outcome of treatment with ruxolitinib in myelofibrosis. *N Engl J Med* **365**, 1455-1457, doi:10.1056/NEJMc1109555 (2011).

16 Verstovsek, S. *et al.* Safety and efficacy of INCB018424, a JAK1 and JAK2 inhibitor, in myelofibrosis. *N Engl J Med* **363**, 1117-1127, doi:10.1056/NEJMoa1002028 (2010).

17 Verstovsek, S. *et al.* Long-term treatment with ruxolitinib for patients with myelofibrosis: 5-year update from the randomized, double-blind, placebo-controlled, phase 3 COMFORT-I trial. *J Hematol Oncol* **10**, 55, doi:10.1186/s13045-017-0417-z (2017).

18 Koppikar, P. *et al.* Heterodimeric JAK-STAT activation as a mechanism of persistence to JAK2 inhibitor therapy. *Nature* **489**, 155-159, doi:10.1038/nature11303 (2012).

19 Rawlings, J. S., Rosler, K. M. & Harrison, D. A. The JAK/STAT signaling pathway. *J Cell Sci* **117**, 1281-1283, doi:10.1242/jcs.00963 (2004).

20 Klampfl, T. *et al.* Somatic mutations of calreticulin in myeloproliferative neoplasms. *N Engl J Med* **369**, 2379-2390, doi:10.1056/NEJMoa1311347 (2013).

21 Levine, R. L. *et al.* Activating mutation in the tyrosine kinase JAK2 in polycythemia vera, essential thrombocythemia, and myeloid metaplasia with myelofibrosis. *Cancer Cell* **7**, 387-397, doi:10.1016/j.ccr.2005.03.023 (2005).

22 Pikman, Y. *et al.* MPLW515L is a novel somatic activating mutation in myelofibrosis with myeloid metaplasia. *PLoS Med* **3**, e270, doi:10.1371/journal.pmed.0030270 (2006).

23 Staerk, J. *et al.* An amphipathic motif at the transmembrane-cytoplasmic junction prevents autonomous activation of the thrombopoietin receptor. *Blood* **107**, 1864-1871, doi:10.1182/blood-2005-06-2600 (2006).

24 Nangalia, J. *et al.* Somatic CALR mutations in myeloproliferative neoplasms with nonmutated JAK2. *N Engl J Med* **369**, 2391-2405, doi:10.1056/NEJMoa1312542 (2013).

25 Marty, C. *et al.* Calreticulin mutants in mice induce an MPL-dependent thrombocytosis with frequent progression to myelofibrosis. *Blood* **127**, 1317-1324, doi:10.1182/blood-2015-11-679571 (2016).

26 Pecquet, C. *et al.* Calreticulin mutants as oncogenic rogue chaperones for TpoR and traffic-defective pathogenic TpoR mutants. *Blood* **133**, 2669-2681, doi:10.1182/blood-2018-09-874578 (2019).

27 Sanjuan-Pla, A. *et al.* Platelet-biased stem cells reside at the apex of the haematopoietic stem-cell hierarchy. *Nature* **502**, 232-236, doi:10.1038/nature12495 (2013).

28 Bianchi, E., Norfo, R., Pennucci, V., Zini, R. & Manfredini, R. Genomic landscape of megakaryopoiesis and platelet function defects. *Blood* **127**, 1249-1259, doi:10.1182/blood-2015-07-607952 (2016).

29 Stachura, D. L., Chou, S. T. & Weiss, M. J. Early block to erythromegakaryocytic development conferred by loss of transcription factor GATA-1. *Blood* **107**, 87-97, doi:10.1182/blood-2005-07-2740 (2006).

30 Wang, X. *et al.* Control of megakaryocyte-specific gene expression by GATA-1 and FOG-1: role of Ets transcription factors. *EMBO J* **21**, 5225-5234, doi:10.1093/emboj/cdf527 (2002).

31 Lecine, P., Italiano, J. E., Jr., Kim, S. W., Villeval, J. L. & Shivdasani, R. A. Hematopoietic-specific beta 1 tubulin participates in a pathway of platelet biogenesis dependent on the transcription factor NF-E2. *Blood* **96**, 1366-1373 (2000).

32 Takayama, M. *et al.* Genetic analysis of hierarchical regulation for Gata1 and NF-E2 p45 gene expression in megakaryopoiesis. *Mol Cell Biol* **30**, 2668-2680, doi:10.1128/MCB.01304-09 (2010).

33 Balduini, A. *et al.* In vitro megakaryocyte differentiation and proplatelet formation in Ph-negative classical myeloproliferative neoplasms: distinct patterns in the different clinical phenotypes. *PLoS One* **6**, e21015, doi:10.1371/journal.pone.0021015 (2011).

34 Gilles, L. *et al.* Downregulation of GATA1 drives impaired hematopoiesis in primary myelofibrosis. *J Clin Invest* **127**, 1316-1320, doi:10.1172/JCI82905 (2017).

35 Villeval, J. L. *et al.* High thrombopoietin production by hematopoietic cells induces a fatal myeloproliferative syndrome in mice. *Blood* **90**, 4369-4383 (1997).

36 Vannucchi, A. M. *et al.* Development of myelofibrosis in mice genetically impaired for GATA-1 expression (GATA-1(low) mice). *Blood* **100**, 1123-1132, doi:10.1182/blood-2002-06-1913 (2002).

37 Chagraoui, H. *et al.* Prominent role of TGF-beta 1 in thrombopoietin-induced myelofibrosis in mice. *Blood* **100**, 3495-3503, doi:10.1182/blood-2002-04-1133 (2002).

38 Zingariello, M. *et al.* Characterization of the TGF-beta1 signaling abnormalities in the Gata1low mouse model of myelofibrosis. *Blood* **121**, 3345-3363, doi:10.1182/blood-2012-06-439661 (2013).

39 Mesa, R. A. *et al.* Primary myelofibrosis (PMF), post polycythemia vera myelofibrosis (post-PV MF), post essential thrombocythemia myelofibrosis (post-ET MF), blast phase PMF (PMF-BP): Consensus on terminology by the international working group for myelofibrosis research and treatment (IWG-MRT). *Leuk Res* **31**, 737-740, doi:10.1016/j.leukres.2006.12.002 (2007).

40 Abdulkarim, K. *et al.* AML transformation in 56 patients with Ph- MPD in two well defined populations. *Eur J Haematol* **82**, 106-111, doi:10.1111/j.1600-0609.2008.01163.x (2009).

41 Mesa, R. A. *et al.* Leukemic transformation in myelofibrosis with myeloid metaplasia: a single-institution experience with 91 cases. *Blood* **105**, 973-977, doi:10.1182/blood-2004-07-2864 (2005).

42 Theocharides, A. *et al.* Leukemic blasts in transformed JAK2-V617F-positive myeloproliferative disorders are frequently negative for the JAK2-V617F mutation. *Blood* **110**, 375-379, doi:10.1182/blood-2006-12-062125 (2007).

43 Tam, C. S. *et al.* The natural history and treatment outcome of blast phase BCR-ABL- myeloproliferative neoplasms. *Blood* **112**, 1628-1637, doi:10.1182/blood-2008-02-138230 (2008).

44 Yogarajah, M. & Tefferi, A. Leukemic Transformation in Myeloproliferative Neoplasms: A Literature Review on Risk, Characteristics, and Outcome. *Mayo Clin Proc* **92**, 1118-1128, doi:10.1016/j.mayocp.2017.05.010 (2017).

45 Abdel-Wahab, O. *et al.* Genetic analysis of transforming events that convert chronic myeloproliferative neoplasms to leukemias. *Cancer Res* **70**, 447-452, doi:10.1158/0008-5472.CAN-09-3783 (2010).

46 Puda, A. *et al.* Frequent deletions of JARID2 in leukemic transformation of chronic myeloid malignancies. *Am J Hematol* **87**, 245-250, doi:10.1002/ajh.22257 (2012).

47 Rampal, R. *et al.* Genomic and functional analysis of leukemic transformation of myeloproliferative neoplasms. *Proc Natl Acad Sci U S A* **111**, E5401-5410, doi:10.1073/pnas.1407792111 (2014).

48 Finazzi, G. *et al.* Acute leukemia in polycythemia vera: an analysis of 1638 patients enrolled in a prospective observational study. *Blood* **105**, 2664-2670, doi:10.1182/blood-2004-09-3426 (2005).

49 Gangat, N. *et al.* Leucocytosis in polycythaemia vera predicts both inferior survival and leukaemic transformation. *Br J Haematol* **138**, 354-358, doi:10.1111/j.1365-2141.2007.06674.x (2007).

50 Tefferi, A. *et al.* Targeted deep sequencing in polycythemia vera and essential thrombocythemia. *Blood Adv* **1**, 21-30, doi:10.1182/bloodadvances.2016000216 (2016).

51 Barbui, T., Thiele, J., Vannucchi, A. M. & Tefferi, A. Problems and pitfalls regarding WHO-defined diagnosis of early/prefibrotic primary myelofibrosis versus essential thrombocythemia. *Leukemia* **27**, 1953-1958, doi:10.1038/leu.2013.74 (2013).

52 Guglielmelli, P. *et al.* Presentation and outcome of patients with 2016 WHO diagnosis of prefibrotic and overt primary myelofibrosis. *Blood* **129**, 3227-3236, doi:10.1182/blood-2017-01-761999 (2017).

53 Chim, C. S. *et al.* Long-term outcome of 231 patients with essential thrombocythemia: prognostic factors for thrombosis, bleeding, myelofibrosis, and leukemia. *Arch Intern Med* **165**, 2651-2658, doi:10.1001/archinte.165.22.2651 (2005).

54 Passamonti, F. *et al.* Prognostic factors for thrombosis, myelofibrosis, and leukemia in essential thrombocythemia: a study of 605 patients. *Haematologica* **93**, 1645-1651, doi:10.3324/haematol.13346 (2008).

55 Barbui, T. *et al.* Survival and disease progression in essential thrombocythemia are significantly influenced by accurate morphologic diagnosis: an international study. *J Clin Oncol* **29**, 3179-3184, doi:10.1200/JCO.2010.34.5298 (2011).

56 Palandri, F. *et al.* Long-term follow-up of 386 consecutive patients with essential thrombocythemia: safety of cytoreductive therapy. *Am J Hematol* **84**, 215-220, doi:10.1002/ajh.21360 (2009).

57 Cervantes, F. *et al.* Acute transformation in nonleukemic chronic myeloproliferative disorders: actuarial probability and main characteristics in a series of 218 patients. *Acta Haematol* **85**, 124-127, doi:10.1159/000204873 (1991).

58 Huang, J. *et al.* Risk factors for leukemic transformation in patients with primary myelofibrosis. *Cancer* **112**, 2726-2732, doi:10.1002/cncr.23505 (2008).

59 Vaidya, R. *et al.* Monosomal karyotype in primary myelofibrosis is detrimental to both overall and leukemia-free survival. *Blood* **117**, 5612-5615, doi:10.1182/blood-2010-11-320002 (2011).

60 Tefferi, A. *et al.* Long-term survival and blast transformation in molecularly annotated essential thrombocythemia, polycythemia vera, and myelofibrosis. *Blood* **124**, 2507-2513; quiz 2615, doi:10.1182/blood-2014-05-579136 (2014).

61 Yoo, L. I., Chung, D. C. & Yuan, J. LKB1--a master tumour suppressor of the small intestine and beyond. *Nat Rev Cancer* **2**, 529-535, doi:10.1038/nrc843 (2002).

62 Tiainen, M., Vaahtomeri, K., Ylikorkala, A. & Makela, T. P. Growth arrest by the LKB1 tumor suppressor: induction of p21(WAF1/CIP1). *Hum Mol Genet* **11**, 1497-1504, doi:10.1093/hmg/11.13.1497 (2002).

63 Boudeau, J. *et al.* MO25alpha/beta interact with STRADalpha/beta enhancing their ability to bind, activate and localize LKB1 in the cytoplasm. *EMBO J* **22**, 5102-5114, doi:10.1093/emboj/cdg490 (2003).

64 Boudeau, J. *et al.* Analysis of the LKB1-STRAD-MO25 complex. *J Cell Sci* **117**, 6365-6375, doi:10.1242/jcs.01571 (2004).

65 Baas, A. F. *et al.* Activation of the tumour suppressor kinase LKB1 by the STE20-like pseudokinase STRAD. *EMBO J* **22**, 3062-3072, doi:10.1093/emboj/cdg292 (2003).

66 Sapkota, G. P. *et al.* Identification and characterization of four novel phosphorylation sites (Ser31, Ser325, Thr336 and Thr366) on LKB1/STK11, the protein kinase mutated in Peutz-Jeghers cancer syndrome. *Biochem J* **362**, 481-490, doi:10.1042/0264-6021:3620481 (2002).

67 Zheng, X. *et al.* Aurora-A-mediated phosphorylation of LKB1 compromises LKB1/AMPK signaling axis to facilitate NSCLC growth and migration. *Oncogene* **37**, 502-511, doi:10.1038/onc.2017.354 (2018).

68 Lee, S. W. *et al.* Skp2-dependent ubiquitination and activation of LKB1 is essential for cancer cell survival under energy stress. *Mol Cell* **57**, 1022-1033, doi:10.1016/j.molcel.2015.01.015 (2015).

69 Konen, J. *et al.* LKB1 kinase-dependent and -independent defects disrupt polarity and adhesion signaling to drive collagen remodeling during invasion. *Mol Biol Cell* **27**, 1069-1084, doi:10.1091/mbc.E15-08-0569 (2016).

70 Wilkinson, S. *et al.* Coordinated cell motility is regulated by a combination of LKB1 farnesylation and kinase activity. *Sci Rep* **7**, 40929, doi:10.1038/srep40929 (2017).

71 Hawley, S. A. *et al.* Complexes between the LKB1 tumor suppressor, STRAD alpha/beta and MO25 alpha/beta are upstream kinases in the AMP-activated protein kinase cascade. *J Biol* **2**, 28, doi:10.1186/1475-4924-2-28 (2003).

72 Shaw, R. J. *et al.* The tumor suppressor LKB1 kinase directly activates AMP-activated kinase and regulates apoptosis in response to energy stress. *Proc Natl Acad Sci U S A* **101**, 3329-3335, doi:10.1073/pnas.0308061100 (2004).

73 Woods, A. *et al.* LKB1 is the upstream kinase in the AMP-activated protein kinase cascade. *Curr Biol* **13**, 2004-2008, doi:10.1016/j.cub.2003.10.031 (2003).

74 Hong, S. P., Leiper, F. C., Woods, A., Carling, D. & Carlson, M. Activation of yeast Snf1 and mammalian AMP-activated protein kinase by upstream kinases. *Proc Natl Acad Sci U S A* **100**, 8839-8843, doi:10.1073/pnas.1533136100 (2003).

75 Nath, N., McCartney, R. R. & Schmidt, M. C. Yeast Pak1 kinase associates with and activates Snf1. *Mol Cell Biol* **23**, 3909-3917, doi:10.1128/mcb.23.11.3909-3917.2003 (2003).

76 Sutherland, C. M. *et al.* Elm1p is one of three upstream kinases for the Saccharomyces cerevisiae SNF1 complex. *Curr Biol* **13**, 1299-1305, doi:10.1016/s0960-9822(03)00459-7 (2003).

77 Hawley, S. A. *et al.* Calmodulin-dependent protein kinase kinase-beta is an alternative upstream kinase for AMP-activated protein kinase. *Cell Metab* **2**, 9-19, doi:10.1016/j.cmet.2005.05.009 (2005).

78 Momcilovic, M., Hong, S. P. & Carlson, M. Mammalian TAK1 activates Snf1 protein kinase in yeast and phosphorylates AMP-activated protein kinase in vitro. *J Biol Chem* **281**, 25336-25343, doi:10.1074/jbc.M604399200 (2006).

79 Kemphues, K. J., Priess, J. R., Morton, D. G. & Cheng, N. S. Identification of genes required for cytoplasmic localization in early C. elegans embryos. *Cell* **52**, 311-320, doi:10.1016/s0092-8674(88)80024-2 (1988).

80 Drewes, G. MARKing tau for tangles and toxicity. *Trends Biochem Sci* **29**, 548-555, doi:10.1016/j.tibs.2004.08.001 (2004).

81 Mohseni, M. *et al.* A genetic screen identifies an LKB1-MARK signalling axis controlling the Hippo-YAP pathway. *Nat Cell Biol* **16**, 108-117, doi:10.1038/ncb2884 (2014).

82 Kishi, M., Pan, Y. A., Crump, J. G. & Sanes, J. R. Mammalian SAD kinases are required for neuronal polarization. *Science* **307**, 929-932, doi:10.1126/science.1107403 (2005).

83 Crump, J. G., Zhen, M., Jin, Y. & Bargmann, C. I. The SAD-1 kinase regulates presynaptic vesicle clustering and axon termination. *Neuron* **29**, 115-129, doi:10.1016/s0896-6273(01)00184-2 (2001).

84 Bright, N. J., Carling, D. & Thornton, C. Investigating the regulation of brain-specific kinases 1 and 2 by phosphorylation. *J Biol Chem* **283**, 14946-14954, doi:10.1074/jbc.M710381200 (2008).
85 Sun, X., Gao, L., Chien, H. Y., Li, W. C. & Zhao, J. The regulation and function of the NUAK family. *J Mol Endocrinol* **51**, R15-22, doi:10.1530/JME-13-0063 (2013).
86 Jaleel, M. *et al.* The ubiquitin-associated domain of AMPK-related kinases regulates conformation and LKB1-mediated phosphorylation and activation. *Biochem J* **394**, 545-555, doi:10.1042/BJ20051844 (2006).
87 Suzuki, A. *et al.* ARK5 suppresses the cell death induced by nutrient starvation and death receptors via inhibition of caspase 8 activation, but not by chemotherapeutic agents or UV irradiation. *Oncogene* **22**, 6177-6182, doi:10.1038/sj.onc.1206899 (2003).
88 Suzuki, A. *et al.* Identification of a novel protein kinase mediating Akt survival signaling to the ATM protein. *J Biol Chem* **278**, 48-53, doi:10.1074/jbc.M206025200 (2003).
89 Fisher, J. S. *et al.* Muscle contractions, AICAR, and insulin cause phosphorylation of an AMPK-related kinase. *Am J Physiol Endocrinol Metab* **289**, E986-992, doi:10.1152/ajpendo.00335.2004 (2005).
90 Wang, Z., Takemori, H., Halder, S. K., Nonaka, Y. & Okamoto, M. Cloning of a novel kinase (SIK) of the SNF1/AMPK family from high salt diet-treated rat adrenal. *FEBS Lett* **453**, 135-139, doi:10.1016/s0014-5793(99)00708-5 (1999).
91 Muraoka, M. *et al.* Involvement of SIK2/TORC2 signaling cascade in the regulation of insulin-induced PGC-1alpha and UCP-1 gene expression in brown adipocytes. *Am J Physiol Endocrinol Metab* **296**, E1430-1439, doi:10.1152/ajpendo.00024.2009 (2009).
92 Du, W. Q., Zheng, J. N. & Pei, D. S. The diverse oncogenic and tumor suppressor roles of salt-inducible kinase (SIK) in cancer. *Expert Opin Ther Targets* **20**, 477-485, doi:10.1517/14728222.2016.1101452 (2016).
93 Tarumoto, Y. *et al.* LKB1, Salt-Inducible Kinases, and MEF2C Are Linked Dependencies in Acute Myeloid Leukemia. *Mol Cell* **69**, 1017-1027 e1016, doi:10.1016/j.molcel.2018.02.011 (2018).
94 Cossette, S. M. *et al.* Sucrose non-fermenting related kinase enzyme is essential for cardiac metabolism. *Biol Open* **4**, 48-61, doi:10.1242/bio.20149811 (2014).
95 Li, J. *et al.* Dysregulation of PP2A-Akt interaction contributes to Sucrose non-fermenting related kinase (SNRK) deficiency induced insulin resistance in adipose tissue. *Mol Metab* **28**, 26-35, doi:10.1016/j.molmet.2019.07.009 (2019).
96 Thirugnanam, K. *et al.* Cardiomyocyte-Specific Snrk Prevents Inflammation in the Heart. *J Am Heart Assoc* **8**, e012792, doi:10.1161/JAHA.119.012792 (2019).
97 Lu, Q. *et al.* Circulating miR-103a-3p contributes to angiotensin II-induced renal inflammation and fibrosis via a SNRK/NF-kappaB/p65 regulatory axis. *Nat Commun* **10**, 2145, doi:10.1038/s41467-019-10116-0 (2019).

98 Utsunomiya, J., Gocho, H., Miyanaga, T., Hamaguchi, E. & Kashimure, A. Peutz-Jeghers syndrome: its natural course and management. *Johns Hopkins Med J* **136**, 71-82 (1975).

99 Giardiello, F. M. *et al.* Very high risk of cancer in familial Peutz-Jeghers syndrome. *Gastroenterology* **119**, 1447-1453, doi:10.1053/gast.2000.20228 (2000).

100 Hearle, N. *et al.* Frequency and spectrum of cancers in the Peutz-Jeghers syndrome. *Clin Cancer Res* **12**, 3209-3215, doi:10.1158/1078-0432.CCR-06-0083 (2006).

101 Hemminki, A. *et al.* A serine/threonine kinase gene defective in Peutz-Jeghers syndrome. *Nature* **391**, 184-187, doi:10.1038/34432 (1998).

102 Jenne, D. E. *et al.* Peutz-Jeghers syndrome is caused by mutations in a novel serine threonine kinase. *Nat Genet* **18**, 38-43, doi:10.1038/ng0198-38 (1998).

103 Volikos, E. *et al.* LKB1 exonic and whole gene deletions are a common cause of Peutz-Jeghers syndrome. *J Med Genet* **43**, e18, doi:10.1136/jmg.2005.039875 (2006).

104 Fulcheri, E., Baracchini, P., Pagani, A., Lapertosa, G. & Bussolati, G. Significance of the smooth muscle cell component in Peutz-Jeghers and juvenile polyps. *Hum Pathol* **22**, 1136-1140, doi:10.1016/0046-8177(91)90266-r (1991).

105 Bardeesy, N. *et al.* Loss of the Lkb1 tumour suppressor provokes intestinal polyposis but resistance to transformation. *Nature* **419**, 162-167, doi:10.1038/nature01045 (2002).

106 Katajisto, P. *et al.* LKB1 signaling in mesenchymal cells required for suppression of gastrointestinal polyposis. *Nat Genet* **40**, 455-459, doi:10.1038/ng.98 (2008).

107 Barta, J. A., Powell, C. A. & Wisnivesky, J. P. Global Epidemiology of Lung Cancer. *Ann Glob Health* **85**, doi:10.5334/aogh.2419 (2019).

108 Matsumoto, S. *et al.* Prevalence and specificity of LKB1 genetic alterations in lung cancers. *Oncogene* **26**, 5911-5918, doi:10.1038/sj.onc.1210418 (2007).

109 Ji, H. *et al.* LKB1 modulates lung cancer differentiation and metastasis. *Nature* **448**, 807-810, doi:10.1038/nature06030 (2007).

110 Li, F. *et al.* LKB1 Inactivation Elicits a Redox Imbalance to Modulate Non-small Cell Lung Cancer Plasticity and Therapeutic Response. *Cancer Cell* **27**, 698-711, doi:10.1016/j.ccell.2015.04.001 (2015).

111 Wingo, S. N. *et al.* Somatic LKB1 mutations promote cervical cancer progression. *PLoS One* **4**, e5137, doi:10.1371/journal.pone.0005137 (2009).

112 Contreras, C. M. *et al.* Loss of Lkb1 provokes highly invasive endometrial adenocarcinomas. *Cancer Res* **68**, 759-766, doi:10.1158/0008-5472.CAN-07-5014 (2008).

113 Contreras, C. M. *et al.* Lkb1 inactivation is sufficient to drive endometrial cancers that are aggressive yet highly responsive to mTOR inhibitor monotherapy. *Dis Model Mech* **3**, 181-193, doi:10.1242/dmm.004440 (2010).

114 Sahin, F. *et al.* Loss of Stk11/Lkb1 expression in pancreatic and biliary neoplasms. *Mod Pathol* **16**, 686-691, doi:10.1097/01.MP.0000075645.97329.86 (2003).

115 Hingorani, S. R. *et al.* Preinvasive and invasive ductal pancreatic cancer and its early detection in the mouse. *Cancer Cell* **4**, 437-450, doi:10.1016/s1535-6108(03)00309-x (2003).

116 Morton, J. P. *et al.* LKB1 haploinsufficiency cooperates with Kras to promote pancreatic cancer through suppression of p21-dependent growth arrest. *Gastroenterology* **139**, 586-597, 597 e581-586, doi:10.1053/j.gastro.2010.04.055 (2010).

117 Gan, B. *et al.* Lkb1 regulates quiescence and metabolic homeostasis of haematopoietic stem cells. *Nature* **468**, 701-704, doi:10.1038/nature09595 (2010).

118 Gurumurthy, S. *et al.* The Lkb1 metabolic sensor maintains haematopoietic stem cell survival. *Nature* **468**, 659-663, doi:10.1038/nature09572 (2010).

119 Nakada, D., Saunders, T. L. & Morrison, S. J. Lkb1 regulates cell cycle and energy metabolism in haematopoietic stem cells. *Nature* **468**, 653-658, doi:10.1038/nature09571 (2010).

120 Wen, Q. J. *et al.* Targeting megakaryocytic-induced fibrosis in myeloproliferative neoplasms by AURKA inhibition. *Nat Med* **21**, 1473-1480, doi:10.1038/nm.3995 (2015).

121 Wen, Q. *et al.* Identification of regulators of polyploidization presents therapeutic targets for treatment of AMKL. *Cell* **150**, 575-589, doi:10.1016/j.cell.2012.06.032 (2012).

122 Schepers, K. *et al.* Myeloproliferative neoplasia remodels the endosteal bone marrow niche into a self-reinforcing leukemic niche. *Cell Stem Cell* **13**, 285-299, doi:10.1016/j.stem.2013.06.009 (2013).

123 Kondo, K., Klco, J., Nakamura, E., Lechpammer, M. & Kaelin, W. G., Jr. Inhibition of HIF is necessary for tumor suppression by the von Hippel-Lindau protein. *Cancer Cell* **1**, 237-246, doi:10.1016/s1535-6108(02)00043-0 (2002).

124 Brunelle, J. K. *et al.* Oxygen sensing requires mitochondrial ROS but not oxidative phosphorylation. *Cell Metab* **1**, 409-414, doi:10.1016/j.cmet.2005.05.002 (2005).

125 Klimova, T. & Chandel, N. S. Mitochondrial complex III regulates hypoxic activation of HIF. *Cell Death Differ* **15**, 660-666, doi:10.1038/sj.cdd.4402307 (2008).

126 Hamanaka, R. B., Weinberg, S. E., Reczek, C. R. & Chandel, N. S. The Mitochondrial Respiratory Chain Is Required for Organismal Adaptation to Hypoxia. *Cell Rep* **15**, 451-459, doi:10.1016/j.celrep.2016.03.044 (2016).

127 Orr, A. L. *et al.* Suppressors of superoxide production from mitochondrial complex III. *Nat Chem Biol* **11**, 834-836, doi:10.1038/nchembio.1910 (2015).

128 Wierenga, A. T., Vellenga, E. & Schuringa, J. J. Convergence of hypoxia and TGFbeta pathways on cell cycle regulation in human hematopoietic stem/progenitor cells. *PLoS One* **9**, e93494, doi:10.1371/journal.pone.0093494 (2014).

129 Xu, R. *et al.* 3-[(1S,2S,3R)-2,3-Difluoro-1-hydroxy-7-methylsulfonylindan-4-yl]oxy-5-fluorobenzo nitrile (PT2977), a Hypoxia-Inducible Factor 2alpha (HIF-2alpha)

Inhibitor for the Treatment of Clear Cell Renal Cell Carcinoma. *J Med Chem* **62**, 6876-6893, doi:10.1021/acs.jmedchem.9b00719 (2019).

130 Shorning, B. Y. & Clarke, A. R. Energy sensing and cancer: LKB1 function and lessons learnt from Peutz-Jeghers syndrome. *Semin Cell Dev Biol* **52**, 21-29, doi:10.1016/j.semcdb.2016.02.015 (2016).

131 Faubert, B. *et al.* Loss of the tumor suppressor LKB1 promotes metabolic reprogramming of cancer cells via HIF-1alpha. *Proc Natl Acad Sci U S A* **111**, 2554-2559, doi:10.1073/pnas.1312570111 (2014).

132 Shackelford, D. B. *et al.* mTOR and HIF-1alpha-mediated tumor metabolism in an LKB1 mouse model of Peutz-Jeghers syndrome. *Proc Natl Acad Sci U S A* **106**, 11137-11142, doi:10.1073/pnas.0900465106 (2009).

133 Baumeister, J. *et al.* Hypoxia-inducible factor 1 (HIF-1) is a new therapeutic target in JAK2V617F-positive myeloproliferative neoplasms. *Leukemia*, doi:10.1038/s41375-019-0629-z (2019).

134 Hayashi, Y. *et al.* Pathobiological Pseudohypoxia as a Putative Mechanism Underlying Myelodysplastic Syndromes. *Cancer Discov* **8**, 1438-1457, doi:10.1158/2159-8290.CD-17-1203 (2018).

135 Takubo, K. *et al.* Regulation of the HIF-1alpha level is essential for hematopoietic stem cells. *Cell Stem Cell* **7**, 391-402, doi:10.1016/j.stem.2010.06.020 (2010).

136 Cho, H. *et al.* On-target efficacy of a HIF-2alpha antagonist in preclinical kidney cancer models. *Nature* **539**, 107-111, doi:10.1038/nature19795 (2016).

137 Spahn, P. N. *et al.* PinAPL-Py: A comprehensive web-application for the analysis of CRISPR/Cas9 screens. *Sci Rep* **7**, 15854, doi:10.1038/s41598-017-16193-9 (2017).

138 Gundry, M. C. *et al.* Highly Efficient Genome Editing of Murine and Human Hematopoietic Progenitor Cells by CRISPR/Cas9. *Cell Rep* **17**, 1453-1461, doi:10.1016/j.celrep.2016.09.092 (2016).